

Finite-temperature renormalization of Standard Model coupled with gravity, and its implications for cosmology

I. Y. Park

*Department of Applied Mathematics, Philander Smith University
Little Rock, AR 72202, USA
inyongpark05@gmail.com*

Abstract

Finite-temperature one-loop renormalization of the Standard Model, coupled with dynamic metrics, is conducted in this study. The entire analysis is coherently carried out by using the refined background field method, applied in the spirit of the Coleman-Weinberg technique. The general form of the propagator, introduced in our previous work to facilitate Feynman diagram computation in a general curved background, proves useful in the presence of time-dependent temperature. Its utilization allows for the analysis of a FLRW background to essentially reduce to that of a constant finite-T flat spacetime. Notably, this method also provides an effective tool for addressing one of the longstanding problems in QCD, the Linde problem. The implications of our findings for cosmology, particularly the cosmological constant problem and Hubble tension, are discussed.

1 Introduction

Quantum corrections, while often negligible in the study of astronomical and cosmological phenomena, manifest observable effects under certain circumstances. For such studies, one should, in principle, consider the quantum-level action, i.e., the 1PI action. Even when higher-derivative quantum corrections are deemed negligible, the renormalization of various constants, including the cosmological and Newton's constants, is generally necessary. Similarly, finite-temperature quantum field theory (QFT) [1–3] effects must be taken into account, as they, among other things, induce shifts in coupling constants, thus potentially leading to observable effects. However, until recently, the finite-T QFT effects have not been adequately addressed, at least not in the manner treated in the recent sequels of the present work, despite their a priori significant contributions to various physical quantities. In this work, we lay the foundations for a more systematic analysis of quantum-gravitational finite-temperature effects in the Standard Model [4] [5] and the Standard Model of cosmology [6–8].

Essentially, we quantize the system of the Standard Model (SM) coupled to gravity by employing foliation-based quantization [9–14], a method developed over recent years, and conduct finite-temperature one-loop renormalization. Quantization of the SM in a flat background is well-established. The SM effective potential was computed to two loops long ago [15]. With the inclusion of gravity, the foliation-based approach can be applied. This method has been successfully employed in analyzing a scalar-gravity system [12] as well as an Einstein-Maxwell system [13]. In this work, we apply this method, in a streamlined and pedagogical manner, to the SM coupled with dynamic metric in finite temperature.

The presence of temperature introduces several complications. Notably, it breaks Lorentz symmetry, serving as an example of generalized spontaneous symmetry breaking: the vacuum no longer respects the symmetry. One uncharted complication introduced by the presence of temperature pertains to our ultimate goal of systematically analyzing finite-temperature effects in an FLRW background. The temperature of the FLRW universe is time-dependent, decreasing since the Big Bang. This raises the question of how to deal with finite-T effects since conventional finite-T QFT techniques, designed for dealing with constant temperatures, cannot be applied directly. As we will show, the key lies in the general form of the propagator introduced in [16] to expedite loop analysis in a curved background. With this device, one can essentially repeat the flat-spacetime constant-T QFT analysis.

UV divergences can be calculated by considering the zero-T case. The beta functions are primarily determined by Z factors, which are not influenced by temperature in a renormalization scheme analogous to \overline{MS} .¹ Therefore, the beta function results remain the same as in the zero-T case, allowing us to focus on the temperature-dependent finite terms. Once renormalization is completed, for certain cosmological studies such as the present one, one may consider the leading-order part of the 1PI action in the derivative expansion, which essentially corresponds to the renormalized action with quantum- and finite-T-corrected coupling constants.

In previous sequels [16] [17], finite-temperature contributions to the cosmological constant (CC) were analyzed in a scalar-gravity system. See, e.g., [18] for a review of the CC problem.

¹In a more general renormalization scheme, the Z factors will contain temperature-dependent terms. We will not consider such a scheme in the present work.

The renormalized mass of the scalar field was set to be on the order of the CMB temperature. The motivation behind this was to address the smallness of the CC, a well-known problem. See [19] for a related discussion. This step was further supported by the principle of minimal sensitivity [20]. In the early universe, during the period of high temperature, the CC is not expected to be small [6] like its present value.² This allows for the employment of a renormalization scheme more akin to that of the zero-T analysis for the present work.

A delicate question arises regarding the application of the renormalization group. It concerns whether one can always consider, given one’s chosen renormalization conditions, the entire range of the energy scale, from the CMB temperature scale to the Planck scale. It may not be possible, even in the absence of beyond-SM physics in the range. Instead, it may be necessary to consider certain renormalization conditions with a specific segment of the energy range. For instance, in addressing the low-energy and CC problem, it is acceptable to set the mass parameter to be small, on the order of the CMB temperature. Suppose one were to find the solutions to the beta functions. The question arises: would it be appropriate to apply these solutions for an energy scale such as the electroweak (EW) scale? The answer is likely to be negative. This is because the setup with the Higgs mass parameter set to be small would not be suitable, or at best, highly inconvenient for addressing physics at such a scale. At low energies, consideration of symmetry restoration is not necessary, hence setting the energy scale μ to be small does not pose any issues. However, this will not be the case for considering EW scale physics. In the present work, we consider a temperature substantially higher than the electroweak scale and adopt an \overline{MS} -like scheme, conceiving renormalization-group running from the electroweak energy scale to an energy scale several orders higher.

A notable technical aspect of our analysis is the Feynman diagrammatic method called the refined background field method (RBFM), applied in the spirit of the Coleman-Weinberg technique. See, e.g., [21] for a review of the Coleman-Weinberg technique. While for a one-loop potential of a relatively simple system, one can rely on the usual method of computing the determinant, this method isn’t always applicable. Furthermore, what is often needed, as is the case here, is the part of the effective action containing derivative terms, rather than the potential. Thus, we predominantly apply the RBFM. Additionally, the tool retains the power of the scalar background covariance even in the presence of temperature, making it a useful asset in handling IR divergences.

The results obtained in the main body have potentially interesting implications for the CC problem, the time dependence of effective coupling constants (especially, the cosmological and Newton’s constants), and the Hubble tension [22] [23]. While the crux argument for our CC-problem-solving proposal was given in earlier sequels, we address a few loose ends here. In those sequels, the potential role of temperature in resolving the Hubble tension was also anticipated. (See [24] for a related discussion.) The finite-T effects must be observable in the CMB power spectrum analysis, as elaborated in the body.

The rest of the paper is organized as follows.

In section 2, we commence with a review of the zero-T flat spacetime one-loop renormal-

²The CC will still turn out to be big due to the finite-T contributions; see below.

ization of the SM. This section serves several purposes, primarily to establish the groundwork for the subsequent analyses, namely the examination of finite-T and graviton contributions. Notably, our computation of the Higgs coupling parameter, β_λ , diverges from the known literature; toward the conclusion of section 2, we address this discrepancy. In section 3, we delve into finite-T analysis, with a focus on the leading-temperature terms. After briefly addressing the UV divergences handled by the zero-T analysis, in section 3.1, we revisit the loop analysis, this time focusing on the IR divergences. Thermal resummation is carried out in both the gauge and fermion sectors in section 3.2, resulting in the acquisition of thermal masses for the gauge and fermion fields. In section 3.3 the Linde problem [25] (see [26] for a review) is revisited, highlighting the potency of our formalism in addressing it. We employ a fermion-loop gauge 2-point amplitude to illustrate the problem and demonstrate that our temperature-driven renormalization scheme, incorporating thermal resummation in the gauge and fermion sectors, can circumvent it. The renormalization scheme proposed in [16], which we also adopt in this work, entails setting m_h to a value approximately around the EW scale, proving instrumental in managing the finite-T infrared divergence. In section 3.4, we undertake the task of enumerating the contributions of gravitons. While their contributions are anticipated to be negligible and not expected to alter the qualitative conclusions drawn from the SM sector analysis, consideration of a curved background is essential, given that a FLRW spacetime, which possesses a time-dependent temperature, *is* a curved background. Moving to section 4, we explore the implications of our findings for cosmology, particularly regarding Hubble tension and time-dependent effective coupling constants, following an elaboration on our previous CC resolution proposal. Concerning Hubble tension, the finite-T effect naturally hints at modifications to cosmological parameters, notably the Hubble constant and Newton’s constant. Numerical analysis is underway to delve deeper into this aspect. The ramifications of the present results for time-dependent effective coupling constants are intriguing, particularly the link between the temperature dependence of the effective CC and that of the effective Newton’s constant, as implied by the quantum-level metric field equation. Finally, in section 5, we summarize our findings and outline several future directions for exploration.

2 Zero-T flat spacetime renormalization

In this section, we begin by examining the renormalization of the Standard Model (SM) in a zero-T flat background, laying the groundwork for subsequent, more complex finite-T analysis in a curved background. The renormalization process in a zero-T flat spacetime for the SM is well established, although there is some confusion, as far as we can tell, regarding the β_λ result (see the remarks at the end of section 2.2) due to different conventions of the SM action. Ultraviolet divergences are determined by a zero-T flat background; however, introducing a nonzero temperature adds layers of complexity, especially in the context of the FLRW background later on. We utilize common steps for computing a given diagram in both zero-T and finite-T cases. Rather than solely presenting final results, we select several diagrams in the zero-T analysis and provide more detailed steps, which can then be applied in the subsequent finite-T analysis. With the zero-T divergences addressed in this section, our focus shifts to the temperature-dependent sectors in Section 3. Throughout this process,

we employ the refined background field method (RBFM), a review of which can be found in [14], and adopt a mostly plus metric.

2.1 The setup

The objective of both the present and subsequent sections is to derive the renormalized form of the action at finite temperature. This process unfolds in several steps. Initially, we revisit the analysis at zero temperature. The electroweak sector of the Standard Model action consists of the following components:

$$\mathcal{L} = \mathcal{L}_{gauge+gh} + \mathcal{L}_{fer} + \mathcal{L}_{Yukawa} + \mathcal{L}_{Higgs}. \quad (1)$$

Each sector is given as follows. The gauge sector is

$$\mathcal{L}_{gauge} = -\frac{1}{4}W_{\mu\nu}^i W^{\mu\nu i} - \frac{1}{4}B_{\mu\nu}B^{\mu\nu} \quad (2)$$

with

$$W_{\mu\nu}^a = \partial_\mu W_\nu^a - \partial_\nu W_\mu^a + gf_{abc}W_\mu^b W_\nu^c, \quad B_{\mu\nu} = \partial_\mu B_\nu - \partial_\nu B_\mu \quad (3)$$

where W_μ^a, B_μ denote $SU(2) \times U(1)$ gauge fields. The ghost action for the $SU(2)$ sector is

$$\mathcal{L}_{gh} = -\partial_\mu c_a^* (\partial^\mu c_a - gf_{abc}W_c^\mu c_b). \quad (4)$$

The fermionic part of the Lagrangian reads:

$$\mathcal{L}_{fer} = -\sum_m^F \left(\bar{q}_{mL} \not{D} q_{mL} + \bar{l}_{mL} \not{D} l_{mL} + \bar{u}_{mR} \not{D} u_{mR} + \bar{d}_{mR} \not{D} d_{mR} + \bar{e}_{mR} \not{D} e_{mR} + \bar{\nu}_{mR} \not{D} \nu_{mR} \right) \quad (5)$$

where

$$\bar{\psi}_{L,R} = (\psi_{L,R})^\dagger i\gamma^0, \quad \psi_{L,R} = P_{L,R} \psi, \quad P_L = \frac{1}{2}(1 - \gamma^5), \quad P_R = \frac{1}{2}(1 + \gamma^5). \quad (6)$$

The symbol ψ collectively denotes the fermionic fields. The covariant derivatives of the fermions are given by

$$\begin{aligned} D_\mu q_{mL\alpha} &= \left[\left(\partial_\mu I - \frac{ig}{2} \vec{\tau} \cdot \vec{W}_\mu - ig' Y_L B_\mu \right) \delta_{\alpha\beta} \right] \begin{pmatrix} u_{mL\beta} \\ d_{mL\beta} \end{pmatrix} \\ D_\mu u_{mR\alpha} &= \left[\left(\partial_\mu I - ig' Y_R B_\mu \right) \delta_{\alpha\beta} \right] u_{mR\beta} \end{aligned} \quad (7)$$

where τ denotes Pauli matrices. For the multiplet $(u_i, d_i, \nu_i, e_i)^T$ where i is the generation index, the values of the hypercharge are

$$Y_L = \left(\frac{1}{6}, \frac{1}{6}, -\frac{1}{2}, -\frac{1}{2} \right), \quad Y_R = \left(\frac{2}{3}, -\frac{1}{3}, 0, -1 \right). \quad (8)$$

The quark Yukawa sector is given by

$$\mathcal{L}_{Yukawa} = -Y_{mn}^d \bar{q}_L^m \Phi d_R^n - Y_{mn}^u \bar{q}_L^m \tilde{\Phi} u_R^n + h.c. \quad (9)$$

The covariant derivative of the scalar is given by

$$D_\mu \Phi = \left(\partial_\mu - \frac{g}{2} i \vec{\tau} \cdot \vec{W}_\mu - \frac{ig'}{2} B_\mu \right) \Phi \quad (10)$$

with

$$\Phi = \begin{pmatrix} \Phi^+ \\ \Phi^0 \end{pmatrix}, \quad \tilde{\Phi} \equiv i\tau_2 \Phi^\dagger = \begin{pmatrix} \Phi^{0\dagger} \\ -\Phi^- \end{pmatrix}, \quad \Phi^2 \equiv \Phi^\dagger \Phi = \Phi^- \Phi^+ + \Phi^{0\dagger} \Phi^0 \quad (11)$$

where $\tau_2 = \begin{pmatrix} 0 & -i \\ i & 0 \end{pmatrix}$. The leptonic sector Lagrangian is given similarly. The Higgs sector is

$$\mathcal{L}_{Higgs} = -(D_\mu \Phi)^\dagger (D^\mu \Phi) - \frac{\lambda}{6} \left(\Phi^2 - \frac{3}{\lambda} \tilde{\mu}^2 \right)^2 \quad (12)$$

where the numerical coefficients of the potential term are chosen for canonical normalization of the kinetic and quartic potential terms of ϕ that appear in the following parametrization,

$$\Phi = \begin{pmatrix} v^+ \\ \frac{\phi + i\zeta}{\sqrt{2}} \end{pmatrix} \quad (13)$$

where v^+ , $v^- (\equiv (v^+)^\dagger)$, ζ are Goldstone bosons. The above form of the parametrization will be explicitly used for some part of the analysis, such as Higgs mass analysis. With the parametrization, the Lagrangian (12) reads

$$\mathcal{L}_{Higgs} = -\partial_\mu v^- \partial^\mu v^+ - \frac{1}{2} \partial_\mu \phi \partial^\mu \phi - \frac{1}{2} \partial_\mu \zeta \partial^\mu \zeta - \frac{\lambda}{6} \left[\frac{1}{2} (2v^- v^+ + \phi^2 + \zeta^2) - \frac{3}{\lambda} \tilde{\mu}^2 \right]^2 \quad (14)$$

For later purposes, let us compute the mass term by focusing on the ϕ field. By shifting $\phi \rightarrow \phi + \tilde{\mu} \sqrt{\frac{6}{\lambda}}$ one gets, for the mass term,

$$-\frac{\lambda}{6} \left[\frac{1}{2} \left(\phi + \tilde{\mu} \sqrt{\frac{6}{\lambda}} \right)^2 - \frac{3}{\lambda} \tilde{\mu}^2 \right]^2 \rightarrow -\frac{\lambda}{6} \tilde{\mu}^2 \frac{6}{\lambda} \phi^2 = -\tilde{\mu}^2 \phi^2 = -\frac{m_h^2}{2} \phi^2 \quad (15)$$

where in the last equality we have defined

$$m_h^2 \equiv 2\tilde{\mu}^2. \quad (16)$$

After giving a vev to the Higgs field, the broken phase gauge fields are defined through

$$\begin{aligned} Z_\mu &\equiv \cos \theta_w W_\mu^3 - \sin \theta_w B_\mu \\ A_\mu &\equiv \sin \theta_w W_\mu^3 + \cos \theta_w B_\mu \end{aligned} \quad (17)$$

where θ_W denotes the Weinberg angle. One also introduces complex gauge fields:

$$W^+ = \frac{1}{\sqrt{2}}(W_\mu^1 - iW_\mu^2) \quad , \quad W^- = \frac{1}{\sqrt{2}}(W_\mu^1 + iW_\mu^2). \quad (18)$$

As for the gauge group generators, we adopt

$$\sum_a \tau_{ij}^a \tau_{kl}^a = 2(\delta_{il}\delta_{kj} - \frac{1}{2}\delta_{ij}\delta_{kl}) \quad , \quad \text{tr}(\tau^a \tau^b) = \tilde{C}_2 \delta^{ab} \quad , \quad \tau^a \tau^a = C_2 \mathbf{1}. \quad (19)$$

Above, $\tilde{C}_2 = 2$ and $C_2 = 3$ for $SU(2)$. We employ dimensional regularization, where an energy scale is introduced through the coupling constants in the following manner:

$$g \rightarrow g\mu^\epsilon, \quad g' \rightarrow g'\mu^\epsilon, \quad y_t \rightarrow y_t\mu^\epsilon, \quad \lambda \rightarrow \lambda\mu^{2\epsilon}. \quad (20)$$

The coupling y_t denotes top Yukawa coupling constant. Let us illustrate the setup of RBFM with the Higgs scalar field. One first shifts

$$\phi \equiv \phi_q + \phi_B, \quad (21)$$

where ϕ_q, ϕ_B denote the quantum field and background field, respectively. (The subscript q in ϕ_q will be suppressed in the body.) Conduct another shift

$$\phi_B \rightarrow \phi_B + \phi_v \quad , \quad \phi_v \equiv \tilde{\mu} \sqrt{\frac{6}{\lambda}} \quad (22)$$

where ϕ_v denotes the vacuum expectation value, leading to

$$\phi \equiv \phi_q + \varphi \quad \text{with} \quad \varphi \equiv \phi_B + \phi_v. \quad (23)$$

As indicated, the field φ is a short-hand notation for $\phi_B + \phi_v$; it can also be taken as an overall background field. In other words one can conduct RBFM by treating φ as the background field, thus directly obtaining the 1PI action in terms of φ (and the gauge/fermion background fields). The renormalization constants, Z 's, are introduced according to

$$W_0^\mu \equiv \sqrt{Z_W} W^\mu \quad , \quad B_0^\mu \equiv \sqrt{Z_B} B^\mu \quad , \quad \psi_0 \equiv \sqrt{Z_\psi} \psi \quad , \quad \Phi_0 \equiv \sqrt{Z_\Phi} \Phi \quad , \quad (24)$$

where the subscript 0 denotes bare quantities. Similarly, for the coupling constants, one introduces

$$g_0 = Z_g g \quad , \quad g'_0 = Z_{g'} g' \quad , \quad Y_0 = Z_Y Y \quad , \quad \lambda_0 = Z_\lambda \lambda. \quad (25)$$

For each Z we define ΔZ by

$$Z \equiv 1 + \Delta Z. \quad (26)$$

The computation of various diagrams below entails delicate technical subtleties, primarily due to the rotation of the gauge fields introduced in eq. (17) and especially, the scalar's development of a vacuum expectation value. With the aim of computing the 1PI effective action, we initially employ the broken-phase action at a conceptual level. It is within this

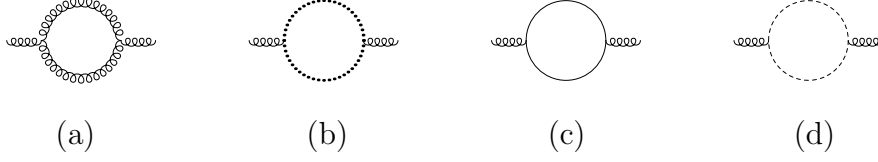


Figure 1: Gauge wavefunction renormalization: (a) gauge loop (b) ghost loop (c) fermion loop (d) scalar loop

framework that the physical significance of various quantities, such as the renormalized Higgs mass parameter, can be properly identified. However, while one could, in principle, utilize the broken action for actual calculations, employing the original unbroken action is technically more straightforward and less tedious due to the preservation of φ -covariance. For most computations, it is more efficient to utilize the original unbroken field basis. This consideration applies to all sectors, but it is particularly advantageous for the scalar sector. Below eq. (46), we will illustrate this point with a scalar-loop two-point diagram.

2.2 One-loop β -functions

For the renormalization of the Higgs mass, it is necessary to first carry out the renormalization of the gauge and fermion fields. We commence with the wave-function renormalization of gauge fields. The relevant diagrams are given in Fig. 1. To elucidate the computation of these diagrams, we provide pedagogical details for (a) and (b). Further elaboration on the refined background field method (RBFM) can be found in [11, 13, 14]. The relevant vertices, following the background shift, stem from

$$\begin{aligned}
-\frac{1}{4}W_{\mu\nu}W^{\mu\nu} \rightarrow & -\frac{g^2}{8}f_{abc}f_{a'b'c'}\left\{\omega_{\mu\nu}^a W_b^\mu W_c^\nu \omega_{\mu'\nu'}^{a'} W_{b'}^{\mu'} W_{c'}^{\nu'} \right. \\
& \left. +4W_{\mu\nu}^a W_\mu^b \omega_\nu^c W_{\mu'\nu'}^{a'} W_{\mu'}^{b'} \omega_{\nu'}^{c'} + 4\omega_{\mu\nu}^a W_b^\mu W_c^\nu W_{\mu'\nu'}^{a'} W_{\mu'}^{b'} \omega_{\nu'}^{c'}\right\}
\end{aligned} \tag{27}$$

where ω denote the background gauge field. Let us examine the contribution of the second term within the curly brackets for illustration purposes. After appropriate contractions of the quantum fields W 's, followed by Fourier transformation and evaluation of the loop momentum integration, the divergent part is obtained as follows:

$$-\frac{\Gamma(\epsilon)}{(4\pi)^2}g^2 f_{abc}f_{a'bc'}\left[\frac{5}{24}p_2^2 \omega^a(p_1) \cdot \omega^{a'}(p_2) - \frac{1}{12}p_2 \cdot \omega^a(p_1) p_2 \cdot \omega^{a'}(p_2)\right]. \tag{28}$$

Above, Γ denotes gamma function and $\epsilon \equiv \frac{4-D}{2}$; p_1, p_2 denote the momenta of the external background fields ω 's. This result cannot be expressed in a gauge-invariant form in position space. However, as anticipated, the sum of all three terms in eq. (27), as well as the ghost diagram, can be shown to be gauge-invariant. By similarly computing the other two terms

and the ghost loop diagram depicted in Fig. 1 (b), the sum is found to be

$$\begin{aligned}
\text{ghost loop} + \text{ghost loop} &= \frac{5}{3} \frac{\Gamma(\epsilon)}{(4\pi)^2} g^2 \left[p_2^2 \omega^a(p_1) \cdot \omega^a(p_2) - p_2 \cdot \omega^a(p_1) p_2 \cdot \omega^a(p_2) \right] \\
&= \frac{5}{6} \frac{\Gamma(\epsilon)}{(4\pi)^2} g^2 \int_x W_{\mu\nu}^a W^{\mu\nu a}
\end{aligned} \tag{29}$$

where $f_{abc}f_{a'bc} = 2\delta_{aa'}$ has been used, and in the second equality, ω is switched back to W for notational convenience. The computation of the fermion diagram in Fig. 1 (c) will be crucial for illustrating our proposal for resolving Linde's problem in the finite-T context. For a fermionic loop, such as an $SU(2)$ quark loop of a specific color and flavor, one obtains

$$\begin{aligned}
\text{fermion loop} &= -g^2 \tilde{C}_2 \int \frac{\delta(p_1 + p_2)}{k^2(k-p_2)^2} \left[k^\mu A_\mu^a(p_1) (k-p_2)^\nu A_\nu^a(p_2) \right. \\
&\quad \left. + (k-p_2)^\mu A_\mu^a(p_1) k^\nu A_\nu^a(p_2) - k_\mu (k-p_2)^\mu A^{a\rho}(p_1) A_\rho^a(p_2) \right]
\end{aligned} \tag{30}$$

where $\delta(p_1 + p_2)$ denotes $(2\pi)^4 \delta(p_1 + p_2)$. This step will be utilized in the subsequent finite-T computation. The total $SU(2)$ fermions, including quarks and leptons, yield

$$\text{fermion loop} |_{\text{quarks + leptons}} = -\frac{\tilde{C}_2}{2} \frac{\Gamma(\epsilon)}{(4\pi)^2} g^2 \int_x W_{\mu\nu}^a W^{\mu\nu a}. \tag{31}$$

The computation of the scalar loop diagram Fig. 1 (d) is summarized as follows:

$$\text{scalar loop} = -\frac{\Gamma(\epsilon)}{(4\pi)^2} g^2 \frac{\tilde{C}_2}{48} \int_x W_{\mu\nu}^a W^{\mu\nu a} - \frac{\Gamma(\epsilon)}{(4\pi)^2} g^2 \frac{\tilde{C}_2}{4} m_h^2 \int_x W_\mu^a W^{a\mu} \tag{32}$$

where m_h denotes the mass of the broken phase, as given in (16). (In the present framework, based on the unbroken basis, the mass m_h arises at the final stage when symmetry breaking is considered. See the comments below eq. (45) and in the introduction of Section 3.) Note that a gauge field mass term is generated; refer to the remarks toward the end of this section. This mass term should be considered as part of the renormalization of the gauge boson mass. Noting $\tilde{C}_2 = 2$ and summing all of the contributions above, the total one-loop $W_{\mu\nu}^2$ term is

$$\frac{1}{48} (40 - 48 - 2) \frac{\Gamma(\epsilon)}{(4\pi)^2} g^2 \int_x W_{\mu\nu}^a W^{\mu\nu a} = -\frac{5}{24} \frac{\Gamma(\epsilon)}{(4\pi)^2} g^2 \int_x W_{\mu\nu}^a W^{\mu\nu a}. \tag{33}$$

This implies

$$\Delta Z_W = -\frac{5}{6} \frac{\Gamma(\epsilon)}{(4\pi)^2} g^2. \tag{34}$$

As for Z_B , by going through analogous steps one can show that the divergent part of the 1PI Lagrangian generated by various contributions is

$$\begin{aligned}
&\left(-\frac{2}{24} - \frac{1}{6} - \frac{5}{3} - \frac{1}{2} - 1 \right) \frac{\Gamma(\epsilon)}{(4\pi)^2} g'^2 \left[p_2^2 B_\mu^a(p_1) B^{a\mu}(p_2) - p_2 \cdot B^a(p_1) p_2 \cdot B^a(p_2) \right] \\
&= -\frac{41}{12} g'^2 \left[p_2^2 B_\mu^a(p_1) B^{a\mu}(p_2) - p_2 \cdot B^a(p_1) p_2 \cdot B^a(p_2) \right]
\end{aligned} \tag{35}$$



Figure 2: Fermion wavefunction renormalization

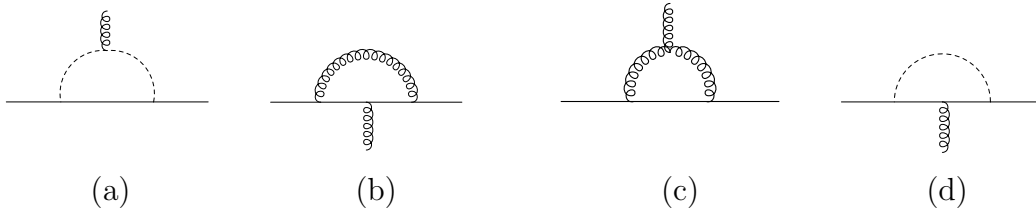


Figure 3: Gauge coupling constant renormalization

where the front factor in the first line represents the contributions from the Higgs, doublet quarks, right-handed quarks, doublet leptons, right-handed leptons, respectively. From this it follows

$$\Delta Z_B = -\frac{41}{6} \frac{\Gamma(\epsilon)}{(4\pi)^2} g'^2. \quad (36)$$

This completes the gauge wavefunction renormalization. Let us consider the fermion wavefunction renormalization. The relevant diagrams are in Fig. 2. Including the factor arising from the color charges one gets

$$\text{---} \overbrace{\text{---}}^{\text{---}} \text{---} = \frac{3}{4} \frac{\Gamma(\epsilon)}{(4\pi)^2} g^2 \bar{q}_L \gamma^\mu \partial_\mu q_L \quad , \quad \text{---} \overbrace{\text{---}}^{\text{---}} \text{---} = -\frac{1}{2} \frac{\Gamma(\epsilon)}{(4\pi)^2} y_t^2 \bar{q}_L \gamma^\mu \partial_\mu q_L \quad (37)$$

where $C_2 = 3$ has been used; y_t denotes the top Yukawa coupling. From these one gets

$$\Delta Z_\psi = -\frac{1}{2} \frac{\Gamma(\epsilon)}{(4\pi)^2} y_t^2 + \frac{3}{4} \frac{\Gamma(\epsilon)}{(4\pi)^2} g^2. \quad (38)$$

As warm-up exercises (and also to verify the consistency of our method), let us compute the beta functions of the gauge sectors. The relevant diagrams are provided in Fig. 3. (The fourth diagram above is relevant only for the case where the gauge line is that of $U(1)$.) For β_g , one may consider either the $A\psi\psi$ vertex or the $AA\Phi\Phi$ vertex where A (ψ) collectively denotes the gauge (fermionic) fields. The fact that they both yield the same result is guaranteed.³ We choose the former for easier comparison with the literature. The

³This is because if one appropriately rescales the gauge field by the (inverse) coupling constant, one obtains an action in which the coupling constant appears as an overall coefficient of the gauge kinetic terms. If one action is renormalizable, the other one should be too, since the two actions are related by a simple gauge field rescaling. The key point is that in the rescaled action, due to covariance, RBFM will produce terms involving $D_\mu \phi^\dagger D^\mu \phi$, so the coupling constant inside will remain unrenormalized, and the renormalization process will mainly affect the covariant kinetic terms. Therefore, in the rescaled action, Z_A and Z_g are not independently determined but only in a certain combination. Once one employs the original action, then Z_A is determined.

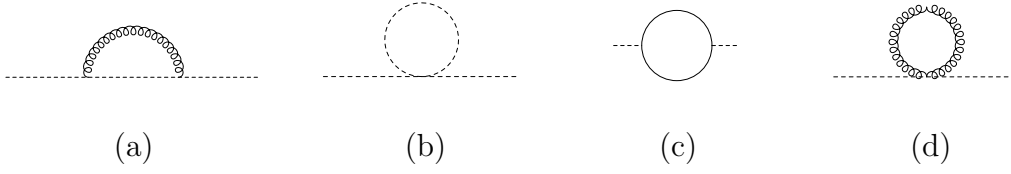


Figure 4: Higgs mass renormalization diagrams.

result of the analysis is summarized as follows:

$$\begin{aligned}
\text{---} \overbrace{\text{---}}^{\text{---}} &= \frac{1}{4} \frac{\Gamma(\epsilon)}{(4\pi)^2} i g y_t^2 \bar{q}_L \tau^a \not{W}^a q_L \\
\text{---} \overbrace{\text{---}}^{\text{---}} &= -\frac{1}{8} g^2 \frac{\Gamma(\epsilon)}{(4\pi)^2} i g \bar{q}_L \tau^a \not{W}^a q_L \\
\text{---} \overbrace{\text{---}}^{\text{---}} &= \frac{3}{4} g^2 \frac{\Gamma(\epsilon)}{(4\pi)^2} i g \bar{q}_L \tau^a \not{W}^a q_L.
\end{aligned} \tag{39}$$

With these one gets

$$\Delta Z_g = -\frac{19}{12} \frac{\Gamma(\epsilon)}{(4\pi)^2} g^2. \tag{40}$$

The beta function β_g is then given by

$$\beta_g = \mu \frac{d}{d\mu} g = -\frac{1}{(4\pi)^2} \frac{19}{6} g^3. \tag{41}$$

Let us turn to $\beta_{g'}$. For an abelian gauge theory, it is well known that the coupling renormalization is determined by that of the wavefunction. The same applies to the abelian sector of the SM:

$$\Delta Z_{g'} = -\frac{1}{2} \Delta Z_B = \frac{41}{12} \frac{\Gamma(\epsilon)}{(4\pi)^2} g'^2 \tag{42}$$

where eq. (36) has been used; one gets

$$\beta_{g'} = \frac{1}{(4\pi)^2} \frac{41}{6} g'^3. \tag{43}$$

With this, Z_g can be determined by utilizing the relation obtained in the rescaled action. (More specifically, consider the original action and determine the wavefunction renormalization. Then consider the coupling terms. Require that the Z_g renormalization renders $D_\mu \phi^\dagger D^\mu \phi$ renormalized only by an overall factor of Z_ϕ .) This, of course, must yield the same result as obtained by solely using the original action.

which, for the φ -dependent part, is the same as (46). The remaining diagrams can be summarized as

$$\begin{aligned}
\text{---}\overbrace{\hspace{1.5cm}}^{\text{---}}\text{---} &= \frac{\Gamma(\epsilon)}{(4\pi)^2}(g^2C_2 + g'^2)\frac{1}{2}\int_x \partial^\mu\Phi^\dagger\partial_\mu\Phi - \frac{\Gamma(\epsilon)}{(4\pi)^2}(g^2C_2 + g'^2)\frac{m_h^2}{4}\int_x \Phi^\dagger\Phi \\
\text{---}\bigcirc\text{---} &= -3y_t^2\frac{\Gamma(\epsilon)}{(4\pi)^2}\int_x \partial^\mu\Phi^\dagger\partial_\mu\Phi \quad , \quad \text{---}\bigcirc\text{---} = 0.
\end{aligned} \tag{50}$$

The gauge-loop diagram above is considered to vanish. This demonstrates the efficacy of applying the RBFM in the spirit of Coleman-Weinberg. These gauge mass-dependent terms can be disregarded because we are considering the Z 's for the unbroken action. At zero temperature, we can primarily rely on the unbroken basis, and that suffices.⁴ The wave-function renormalization constant ΔZ_Φ is determined by

$$-\Delta Z_\Phi\partial_\mu\Phi^\dagger\partial^\mu\Phi + \frac{\Gamma(\epsilon)}{(4\pi)^2}(g^2C_2 + g'^2)\frac{1}{2}\int \partial^\mu\Phi^\dagger\partial_\mu\Phi - 3y_t^2\frac{\Gamma(\epsilon)}{(4\pi)^2}\int \partial^\mu\Phi^\dagger\partial_\mu\Phi = 0 \tag{51}$$

which yields

$$\Delta Z_\Phi = \frac{\Gamma(\epsilon)}{(4\pi)^2}\left[\frac{1}{2}(g^2C_2 + g'^2) - 3y_t^2\right]. \tag{52}$$

The mass renormalization goes:

$$-m_h^2(\Delta Z_{m_h^2} + \Delta Z_\Phi)\Phi^\dagger\Phi - \frac{\Gamma(\epsilon)}{(4\pi)^2}(g^2C_2 + g'^2)\frac{m_h^2}{4}\Phi^\dagger\Phi + m_h^2\lambda\frac{\Gamma(\epsilon)}{(4\pi)^2}\Phi^\dagger\Phi = 0, \tag{53}$$

leading to

$$\Delta Z_{m_h^2} = \frac{\Gamma(\epsilon)}{(4\pi)^2}\left[-\frac{3}{4}(g^2C_2 + g'^2) + \lambda + 3y_t^2\right]. \tag{54}$$

The beta function then reads

$$\beta(m_h^2) = \frac{m_h^2}{(4\pi)^2}\left[-\frac{9}{2}g^2 - \frac{3}{2}g'^2 + 2\lambda + 6y_t^2\right]. \tag{55}$$

This result confirms the corresponding result of Ford et al. (1992) [15].

For the renormalization of the Higgs quartic coupling, the relevant graphs are provided in Fig. 5. (The diagrams obtained by permuting the external lines - which are not shown - are associated with the symmetry factors, which are automatically accounted for in the RBFM formalism.) We illustrate the calculation with diagrams (a) and (b). For diagram (a), there are three different kinds, depending on which of the $SU(2) \times U(1)$ gauge fields runs on the

⁴In other words, it is unnecessary to explicitly consider the Higgs shift to ensure the removal of UV divergences for all non-Higgs sectors. For the Higgs sector on the other hand, it is crucial to focus on the proper Higgs mass term and consider the shift, since our interest lies not in the renormalization of the wrong-sign mass term but in that of the proper Higgs mass term of the broken phase. Consideration of the proper mass term amounts to employing the massive Higgs propagator.

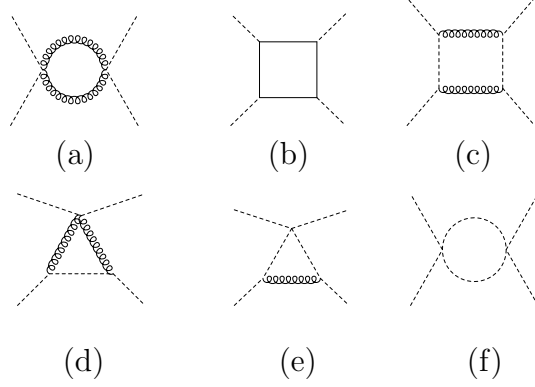


Figure 5: Higgs coupling renormalization. The diagrams with external lines permuted are not included.

loop. Let us consider the case of W -fields running on the loop. After simplification of the initial correlator expression, we obtain

$$\text{Diagram (a)} = \frac{3}{4}g^4 \int_{p',s,k} [\Phi(p_1)^\dagger \Phi(p_2)] [\Phi^\dagger(p_3) \Phi(p_4)] \frac{\delta(\Sigma p_l)}{k^2(k+p_3-p_4)^2} \quad (56)$$

where $\delta(\Sigma p_l)$ denotes $(2\pi)^4 \delta(p_1 + p_3 - p_2 - p_4)$. The finite-T counterpart of this expression will serve as the starting point for the same diagram in the finite-T analysis in section 3. Performing the momentum integrations yields

$$\text{Diagram (a)} = \frac{\Gamma(\epsilon)}{(4\pi)^2} \frac{3}{4} g^4 \int_x (\Phi^\dagger \Phi)^2. \quad (57)$$

Similarly, for diagram (b), one can show, after some algebra,

$$\text{Diagram (b)} = \frac{-y_t^4 (\delta^{\mu\nu} \delta^{\rho\sigma} - \delta^{\mu\rho} \delta^{\nu\sigma} + \delta^{\mu\sigma} \delta^{\nu\rho})}{k^2(k-p_1)^2(k-p_1+p_4)^2(k-p_3)^2} \int_{p',s,k} \Phi_m(p_1) \Phi_n(p_2) \Phi_m^\dagger(p_3) \Phi_n^\dagger(p_4) \delta(\Sigma p_l) \quad (58)$$

where $\delta(\Sigma p_l)$ denotes $(2\pi)^4 \delta(p_1 + p_2 - p_3 - p_4)$. As in the previous diagram, an analogous expression will be the starting point of the same diagram in the finite-temperature analysis. Performing the momentum integrations one gets

$$\text{Diagram (b)} = -\frac{\Gamma(\epsilon)}{(4\pi)^2} 3y_t^4 \int_x (\Phi^\dagger \Phi)^2 \quad (59)$$

where the factor 3 comes from the color index of the fermions. Diagrams (c) - (e) can be similarly computed.

$$\begin{aligned} \text{Diagram (c)} &= \frac{\Gamma(\epsilon)}{(4\pi)^2} \frac{1}{16} g^4 \int_x (\Phi^\dagger \Phi)^2, & \text{Diagram (d)} &= -\frac{\Gamma(\epsilon)}{(4\pi)^2} \frac{5}{8} g^4 \int_x (\Phi^\dagger \Phi)^2 \\ \text{Diagram (e)} &= -\frac{\Gamma(\epsilon)}{(4\pi)^2} \frac{\lambda_s}{4} g^2 \int_x (\Phi^\dagger \Phi)^2. \end{aligned} \quad (60)$$

Finally, consider Fig. 5 (f). By employing the complex basis Feynman diagram method one can show

$$\text{Diagram} = \frac{\Gamma(\epsilon)}{(4\pi)^2} \frac{\lambda^2}{3} \int_x (\Phi^\dagger \Phi)^2. \quad (61)$$

Let us cross-check this result, this time, by employing the real basis Coleman-Weinberg technique. As before, we focus on the φ background field; the relevant ϕ -quadratic part of the potential is given in (45). Each of these vertices on the right-hand side yields φ^4 term with the following sum:

$$\frac{\lambda^2}{12} \frac{\Gamma(\epsilon)}{(4\pi)^2} \int_x \varphi^4 \quad (62)$$

which confirms (61) for the φ^4 part.

One is now ready to tackle renormalization of λ . Adding all of the contributions from Fig. 5 (a)-(f) (and the contributions from the $U(1)$ gauge field as well), one gets

$$\frac{(4\pi)^2}{\Gamma(\epsilon)} 4\lambda \Delta Z_\lambda = 8\lambda^2 - 18\lambda g^2 - 6\lambda g'^2 + 24\lambda y_t^2 + \frac{9}{2}g^4 + 3g^2 g'^2 + \frac{3}{2}g'^4 - 72y_t^4. \quad (63)$$

Requiring the bare coupling's independence of the scale,

$$\mu \frac{d}{d\mu} (\mu^{2\epsilon} Z_\lambda \lambda) = 0 \quad \Rightarrow \quad \frac{\mu}{\lambda} \frac{d}{d\mu} \lambda = -\frac{\mu}{Z_\lambda} \frac{d}{d\mu} Z_\lambda \simeq -\mu \frac{d}{d\mu} Z_\lambda \quad (64)$$

where the last equality is valid in the one-loop approximation. From this it follows

$$\mu \frac{d}{d\mu} Z_\lambda = \frac{\Gamma(\epsilon)}{(4\pi)^2} \mu \frac{d}{d\mu} \left[2\lambda - \frac{9}{2}g^2 - \frac{3}{2}g'^2 + 6y_t^2 + \frac{9}{8} \frac{g^4}{\lambda} + \frac{3}{4} \frac{g^2 g'^2}{\lambda} + \frac{3}{8} \frac{g'^4}{\lambda} - 18 \frac{y_t^4}{\lambda} \right]. \quad (65)$$

The Higgs coupling beta function is then given by

$$\begin{aligned} \beta_\lambda &\equiv \mu \frac{d}{d\mu} \lambda = -\lambda \mu \frac{d}{d\mu} Z_\lambda \\ &\simeq \frac{1}{(4\pi)^2} \left[4\lambda^2 - 9\lambda g^2 - 3\lambda g'^2 + 12\lambda y_t^2 + \frac{9}{4}g^4 + \frac{3}{2}g^2 g'^2 + \frac{3}{4}g'^4 - 36y_t^4 \right]. \end{aligned} \quad (66)$$

Some of the coefficients above do not agree with those of Machacek and Vaughn (1984) [27], as noted in the remarks below.

Remarks:

Let us revisit the following aspects of the analysis above. We have observed that the gauge two-point function with a Higgs loop generates a gauge mass term. In QED, the photon self-energy term does not violate gauge invariance; namely, the photon mass term is not generated. As we have noted, this is not the case for the SM. This may not be a problem for the SM, at least not a serious one, since the gauge mass term comes from the Higgs

mass term, which in turn originates from the spontaneous symmetry breaking: the gauge symmetry is broken anyway. However, this could pose a problem for a scalar QED: although the classical action is gauge invariant, the one-loop self-energy is not. The takeaway should be that the usefulness of a regularization method is theory-dependent.

As for the result (66), let us compare it with the corresponding result in [27] [28] where a different convention, $-\frac{\lambda}{2}\left(\Phi^2-\frac{3}{\lambda}\tilde{\mu}^2\right)^2$, was employed for the quartic potential term:

$$(4\pi)^2\beta_\lambda = 12\lambda^2 - (3g'^2 + 9g^2)\lambda + \frac{9}{4}g^4 + \frac{3}{2}g^2g'^2 + \frac{3}{4}g'^4 + \dots . \quad (67)$$

To make comparison, let us go back to the right-hand side of (64) and rescale it:

$$\Rightarrow \quad \frac{\mu}{\lambda} \frac{d}{d\mu} \lambda = -\mu \frac{d}{d\mu} Z_{3\lambda} \quad (68)$$

from which one gets

$$\begin{aligned} \beta_\lambda &= \mu \frac{d}{d\mu} \lambda = -\mu \lambda \frac{d}{d\mu} Z_{3\lambda} \\ &= \frac{\Gamma(\epsilon)}{(4\pi)^2} \mu \frac{d}{d\mu} \left[6\lambda - \frac{9}{2}g^2 - \frac{3}{2}g'^2 + 6y_t^2 + \frac{3}{8} \frac{g^4}{\lambda} + \frac{1}{4} \frac{g^2g'^2}{\lambda} + \frac{1}{8} \frac{g'^4}{\lambda} - 6 \frac{y_t^4}{\lambda} \right]. \end{aligned} \quad (69)$$

This leads to

$$(4\pi)^2\beta_\lambda = 12\lambda^2 - (3g'^2 + 9g^2)\lambda + \frac{3}{4}g^4 + \frac{1}{2}g^2g'^2 + \frac{1}{4}g'^4 + \dots . \quad (70)$$

This does not agree with the existing result, eq. (67). For instance, the coefficients of the quartic gauge coupling terms in (67) are larger than those in (70) by a factor 3.

3 Finite-temperature renormalization in a curved space-time

With the completion of the zero-T flat spacetime analysis, in this section, we branch out to investigating the constant finite-T effects of the Standard Model (SM) in both a flat and FLRW background. To accurately account for temperature effects in cosmology, it is essential to consider not only the thermodynamics of the hydrodynamic matter but also the finite-T quantum-field-theoretic contributions of the SM fields. We analyze the finite-temperature shifts of coupling constants, which should be regarded as effective coupling "constants." This entrance of effective coupling constants is exemplified by the Higgs mass and coupling constant.

The primary focus here lies on infrared divergence. The combined use of RBFM with the Coleman-Weinberg method proves to be highly beneficial in elucidating the intricate points involved in resolving the IR divergences. As previously employed in the previous section, we utilize the massive Higgs propagator alongside the massless propagators for the gauge and

fermion fields. In this section, these fields are ultimately perceived as having temperature-dependent effective masses. Nonetheless, the starting points of all these seemingly distinct treatments stem from the Coleman-Weinberg-spirit Feynman diagrammatic technique. The apparent differences in treatments merely reflect varying levels of explicitness in the analysis, depending on whether or not the Higgs mass term is explicitly separated from the Higgs background field φ .

In section 3.1, we undertake the flat spacetime constant-T analysis, detailing the thermal resummation in the gauge and fermion sectors. The expressions of the thermal masses of the gauge and fermionic fields introduced thereby are discussed in section 3.2. We observe in section 3.3 that the cause for the Linde problem can be circumvented. Building upon the device proposed in previous work [16, 17], designed to handle loops in a general curved background at zero-T, we find that it can adeptly address the time-dependent temperature complications as well. In section 3.4, we incorporate the graviton sector and note that the loop analysis essentially reduces to the constant-T flat spacetime case. This implies that the insights gleaned from the analysis in section 3.1 extend beyond their immediate application, as even for a FLRW background, one can leverage the results obtained there. A similar relation for a zero-T curved background was highlighted in [16]. The results obtained in the present section harbor potentially intriguing implications for the CC problem, effective coupling constants, and Hubble tension, which are pondered in section 4.

3.1 Finite-T shifts in Higgs mass and coupling

In this section, we employ the perturbative scheme of high-temperature expansion to investigate the finite-temperature behaviors of the Higgs mass and coupling.⁵ Despite the presence of temperature, which breaks Lorentz symmetry (and diffeomorphism symmetry in a curved background), the counter-terms for UV divergences retain the same covariant forms as in the zero-T case, remaining T-independent. This simplifies several aspects of the analysis. While one should ideally consider all diagrams analyzed in the zero-T setup, the renormalization of the Higgs mass and coupling can be addressed without entirely repeating the gauge and fermion sector analyses due to this property.⁶

For the shifts in the Higgs mass and coupling, we reanalyze the diagrams in Fig. 4 and 5 in the finite-T setup. Additionally, we need to consider Fig. 1 (c) to tackle the issue of infrared

⁵In a more general context, beyond one-loop calculations, it becomes necessary to account for the finite T-dependent terms of the kinetic term as well. Incorporating these terms, particularly when computing propagators, effectively results in a form of resummation. The inclusion of such terms becomes crucial depending on the specific problem under investigation, as they can have significant implications for the overall behavior of the system. Therefore, considering these T-dependent finite terms becomes essential for a comprehensive understanding of the system's dynamics, especially in higher-loop calculations.

⁶An intuitive but non-rigorous way to understand how zero-T renormalization handles UV divergences is by considering a low-T expansion. Since the divergence part is independent of temperature, the renormalization procedure at zero temperature should remain unchanged. For the high-T case, one can imagine summing up the low-T series into a closed form. This closed form can then be extrapolated to the high-T regime, implying that the renormalization procedure for high-T scenarios should be identical to that of the low-T case.

However, for a more rigorous discussion and comprehensive understanding, one should refer to the literature, such as [3], which provides detailed analysis and explanations of these concepts.

divergence, which necessitates a separate treatment. We revisit the loop analysis, this time focusing on the IR divergences associated with finite-T effects. These divergences can be circumvented through thermal resummation, which is necessary even though we restrict the analysis to one-loop. When applied to the Higgs sector, thermal resummation results in a thermal Higgs mass proportional to T^2 . Consequently, gauge bosons and fermions will develop mass terms of the same order, leading to several significant implications.

Firstly, the thermal masses enable the resolution of the infrared divergence problem encountered in the computation of some diagrams in Fig. 5. Furthermore, the implications for the Linde problem are noteworthy. The cause of the Linde problem can be attributed to the disregard of quark masses compared to the temperature. In our dynamic temperature-driven mass renormalization scheme, quark masses cannot be disregarded after resummation since they are of the order of the temperature. Applied to QCD, this implies that both the electric and magnetic components of gluons develop thermal mass terms, thus circumventing the Linde problem.

As before, one needs to compute the four diagrams in Fig. 4. The diagrams can be evaluated based on the following well known results (see, e.g., [3]): for a bosonic loop

$$\begin{aligned}
J(m, t) &\equiv \not\int \left[\frac{1}{2} \ln(K^2 + m^2) - const \right] = -\frac{\pi^2}{90} T^4 + \frac{m^2}{24} T^2 - \frac{1}{12\pi} m^3 T \\
&\quad - \frac{\mu^{-2\epsilon}}{2(4\pi)^2} m^4 \left[\ln \left(\frac{\bar{\mu} e^\gamma}{4\pi T} \right) + \frac{1}{2\epsilon} \right] + \frac{\zeta(3)}{3(4\pi)^4} \frac{m^6}{T^2} + \mathcal{O} \left(\frac{m^8}{T^4} \right) + \mathcal{O}(\epsilon) \\
I(m, T) &\equiv \not\int \frac{1}{K^2 + m^2} = \frac{T^2}{12} - \frac{mT}{4\pi} - \frac{2\mu^{-2\epsilon}}{(4\pi)^2} m^2 \left[\ln \left(\frac{\bar{\mu} e^\gamma}{4\pi T} \right) + \frac{1}{2\epsilon} \right] \\
&\quad + \frac{2\zeta(3)}{(4\pi)^4} \frac{m^4}{T^2} + \mathcal{O} \left(\frac{m^6}{T^4} \right) + \mathcal{O}(\epsilon)
\end{aligned} \tag{71}$$

where $\ln \bar{\mu}^2 \equiv \ln(4\pi\mu^2) - \gamma$; γ is an Euler's constant. It is also useful to record the expression of I prior to the large- T expansion:

$$\begin{aligned}
I(m, T) &= T \sum_{n=0} \int \frac{d^d \mathbf{k}}{(2\pi)^d} \frac{1}{\omega_n^2 + \mathbf{k}^2 + m^2} \\
&= \frac{\Gamma(-\frac{1}{2} + \epsilon)}{(4\pi)^{\frac{3}{2} - \epsilon}} T m^{1-2\epsilon} + \frac{1}{2 \pi^{2-\frac{d}{2}} T^{1-d}} \sum_{l=0}^{\infty} \zeta(2l + 2 - d) \frac{\Gamma(l + 1 - \frac{d}{2}) (-1)^l m^{2l}}{\Gamma(l + 1) (2\pi T)^{2l}}.
\end{aligned} \tag{72}$$

Note that in the series term above, the (m, T) -dependence comes only in the form $\frac{m^{2l}}{T^{1-d+2l}}$. For a fermionic loop one instead gets

$$\tilde{J}(m, T) \equiv J_0(m) + \tilde{J}_T(m) \quad , \quad \tilde{I}(m, T) \equiv I_0(m) + \tilde{I}_T(m) \tag{73}$$

where

$$\begin{aligned}
J_0(m) &= -\frac{m^4 \mu^{-2\epsilon}}{64\pi^2} \left[\frac{1}{\epsilon} + \ln \frac{\bar{\mu}^2}{m^2} + \frac{3}{2} + \mathcal{O}(\epsilon) \right] \\
I_0(m) &= -\frac{m^2 \mu^{-2\epsilon}}{16\pi^2} \left[\frac{1}{\epsilon} + \ln \frac{\bar{\mu}^2}{m^2} + 1 + \mathcal{O}(\epsilon) \right]
\end{aligned} \tag{74}$$

and

$$\begin{aligned}
\tilde{J}_T(m) &= \frac{7\pi^2}{890} T^4 - \frac{m^2}{48} T^2 - \frac{1}{2(4\pi)^2} m^4 \left[\ln\left(\frac{me^\gamma}{\pi T}\right) - \frac{3}{4} \right] + \frac{7\zeta(3)}{3(4\pi)^4} \frac{m^6}{T^2} + \dots \\
\tilde{I}_T(m) &= -\frac{T^2}{24} - \frac{2}{(4\pi)^2} m^2 \left[\ln\left(\frac{me^\gamma}{\pi T}\right) - \frac{1}{2} \right] + \frac{14\zeta(3)}{(4\pi)^4} \frac{m^4}{T^2} + \dots
\end{aligned} \tag{75}$$

We can illustrate the finite-T computation with several diagrams. Let us illustrate it with the scalar-loop diagram shown in Fig. 4 (b). This diagram can be computed by applying a finite-T modification of Eq. (48): replacing $\int d^4k$ by \int_x^f , one gets, on account of (71),

$$\text{---} \circ \text{---} = -\lambda \left(\int d^4x \Phi^\dagger \Phi \right) \int_x^f \frac{1}{K^2 + m_h^2} = -\lambda \left(\frac{T^2}{12} - \frac{1}{4\pi} m_h T + \dots \right) \int_x \Phi^\dagger \Phi. \tag{76}$$

The rest of the diagrams can be similarly computed⁷:

$$\begin{aligned}
\text{---} \text{---} \text{---} &= \frac{1}{4} (C_2 g^2 + g'^2) \left(\frac{T^2}{12} - \frac{1}{4\pi} m_h T + \dots \right) \int_x \Phi^\dagger \Phi \\
\text{---} \text{---} \text{---} &= -(C_2 g^2 + g'^2) \left(\frac{T^2}{12} + \dots \right) \int_x \Phi^\dagger \Phi \\
\text{---} \text{---} &= 6y_t^2 \left(-\frac{T^2}{24} + \dots \right) \int_x \Phi^\dagger \Phi.
\end{aligned} \tag{77}$$

Summing up, one gets, at the leading order,

$$\begin{aligned}
&\int_x \left\{ \left[-\lambda + \frac{1}{4} (C_2 g^2 + g'^2) - (C_2 g^2 + g'^2) + 6y_t^2 \right] \frac{T^2}{12} + \dots \right\} \Phi^\dagger \Phi \\
&\simeq \int_x \frac{1}{12} \left[-\lambda - \frac{3}{4} (3g^2 + g'^2) - 3y_t^2 \right] T^2 \Phi^\dagger \Phi
\end{aligned} \tag{78}$$

which confirms the corresponding part of [29]. As for the Higgs coupling renormalization, the zero-T results can again be utilized. However, unlike the mass term, one encounters a complication not present in the zero-T case: the infrared divergence. We illustrate it with the gauge- and fermionic-loop diagrams Fig. 5 (a) and (b). By utilizing (56), the gauge-loop diagram (a) is given by:

$$\text{---} \text{---} \text{---} = \frac{3}{4} g^4 \int_{\{P_1, P_2, P_3, P_4\}}^f \Phi_{P_1}^\dagger \Phi_{P_2} \Phi_{P_3}^\dagger \Phi_{P_4} \delta(\Sigma P_l) \int_x^f \frac{1}{K^2 (K + P_3 - P_4)^2} \tag{79}$$

where $\delta(\Sigma P_l)$ denotes $(2\pi)^4 \delta(P_1 + P_3 - P_2 - P_4)$. Let us evaluate the sum-integral over K^μ . Since we are interested in the potential it is not necessary to keep track of the P -dependent terms. (They will yield terms with derivatives in the position space.) Also, they

⁷The first and fourth diagrams also contribute to kinetic terms. These terms are non-gauge-covariant, yet the breaking effects are subleading in T .

are subleading in the large-temperature expansion. The K -integrand of the above can be expanded as

$$\not\int \frac{1}{K^2(K+P_3-P_4)^2} \simeq \not\int \left(\frac{1}{K^4} - \frac{2(P_3-P_4) \cdot K}{K^6} - \frac{(P_3-P_4)^2}{K^6} \right). \quad (80)$$

Postponing the analysis of the higher order terms, such as $\sim \frac{1}{K^6}$, let us evaluate the first two terms. The second term in (80) vanishes due to the odd parity of the integrand. The leading term $\not\int \frac{1}{K^4}$ can be evaluated by taking $\frac{1}{m} \frac{\partial}{\partial m}$ on $I(m, T)$ followed by a limit $m \rightarrow 0$:

$$\begin{aligned} \not\int \frac{1}{(K^2+m^2)^2} &= -\frac{1}{2m} \left(-\frac{T}{4\pi} - \frac{4\mu^{-2\epsilon}}{(4\pi)^2} m \left[\ln \left(\frac{\bar{\mu} e^\gamma}{4\pi T} \right) + \frac{1}{2\epsilon} \right] + \frac{8\zeta(3)}{(4\pi)^4} \frac{m^3}{T^2} + \dots \right) \\ &= \frac{T}{8\pi m} + \frac{2\mu^{-2\epsilon}}{(4\pi)^2} \left[\ln \left(\frac{\bar{\mu} e^\gamma}{4\pi T} \right) + \frac{1}{2\epsilon} \right] - \frac{4\zeta(3)}{(4\pi)^4} \frac{m^2}{T^2} + \dots \end{aligned} \quad (81)$$

If we take the mass of the gauge fields to be zero as in the zero-T analysis, one encounters a problem as one takes the $m \rightarrow 0$ limit, the well-known infrared divergence problem. The same problem occurs in the fermionic-loop diagram, Fig. 5 (b). By utilizing the zero-T result (58), one gets

$$\begin{aligned} \text{Diagram} &= -y_t^4 (\delta^{\mu\nu} \delta^{\rho\sigma} - \delta^{\mu\rho} \delta^{\nu\sigma} + \delta^{\mu\sigma} \delta^{\nu\rho}) \not\int_{P'_s} \Phi_m(P_1) \Phi_n(P_2) \Phi_m^\dagger(P_3) \Phi_n^\dagger(P_4) \delta(\Sigma P_l) \\ &\quad \tilde{\not\int} \frac{K_\mu K_\nu K_\rho K_\sigma}{K^2(K-P_1)^2(K-P_1+P_4)^2(K-P_3)^2} \end{aligned} \quad (82)$$

where $\delta(\Sigma P_l)$ denotes $(2\pi)^4 \delta(P_1 + P_2 - P_3 - P_4)$. Let us expand the K -integrand:

$$\begin{aligned} &\simeq -y_t^4 \not\int_{P'_s} \Phi_m(P_1) \Phi_n(P_2) \Phi_m^\dagger(P_3) \Phi_n^\dagger(P_4) \delta(\Sigma P_l) \\ &\quad \tilde{\not\int} \left[\frac{1}{K^4} + 2 \frac{(2P_1 - P_4 + P_3) \cdot K}{K^6} - \frac{P_1^2 + (P_1 - P_4)^2 + P_3^2}{K^6} + \dots \right]. \end{aligned} \quad (83)$$

Here again the leading order is $\frac{1}{K^4}$,

$$\tilde{\not\int} \frac{1}{(K^2+m^2)^2} = \frac{\mu^{-2\epsilon}}{(4\pi)^2} \left[\frac{1}{\epsilon} + \ln \frac{\bar{\mu}^2}{m_f^2} + \mathcal{O}(\epsilon) \right] + \frac{2}{(4\pi)^2} \ln \frac{m e^\gamma}{\pi T} - \frac{28\zeta(3)}{(4\pi)^4} \frac{m_f^2}{T^2} \dots \quad (84)$$

Where the tilde above the integral indicates the fermionic sum-integral. As with the bosonic case, one encounters infrared divergence due to the lack of the mass term. The divergence can be avoided by conducting thermal resummation. Let us pause and recapitulate. Since we are interested in one-loop, it is not necessary, though useful anyway, to consider thermal resummation when it comes to ultraviolet divergence. As the example above reveals, however, it is not the case for infrared divergence: the finite-T effects introduce IR divergence, which in turn is solved by (partially⁸ two-loop) finite-T resummation to be spelled out. We will

⁸It is partially two-loop since we are only considering the two-loop coming from the resummation.

shortly discuss how the mass terms of gauge and fermion fields appear, but for now let us temporarily denote the temperature-dependent gauge and fermion mass parameters by

$$(m_g, m_f), \quad (85)$$

respectively, and proceed. The results obtained above now take the form:

$$\begin{aligned} \text{Diagram 1} &= \frac{3}{4}g^4 \left(\not{\int} \frac{1}{(K^2 + m_g^2)^2} + \dots \right) \int_x \Phi^\dagger \Phi \\ &= \frac{3}{4}g^4 \left(-\frac{1}{2m_g} \right) \left(-\frac{T}{4\pi} - \frac{4\mu^{-2\epsilon}}{(4\pi)^2} m_g \left[\ln \left(\frac{\bar{\mu}e^\gamma}{4\pi T} \right) + \frac{1}{2\epsilon} \right] + \frac{8\zeta(3)}{(4\pi)^4} \frac{m_g^3}{T^2} + \dots \right) \int_x \Phi^\dagger \Phi \\ &= \frac{3}{4}g^4 \left\{ \frac{1}{8\pi} \frac{T}{m_g} + \frac{2\mu^{-2\epsilon}}{(4\pi)^2} \left[\ln \left(\frac{\bar{\mu}e^\gamma}{4\pi T} \right) + \frac{1}{2\epsilon} \right] - \frac{4\zeta(3)}{(4\pi)^4} \frac{m_g^2}{T^2} + \dots \right\} \int_x \Phi^\dagger \Phi \end{aligned} \quad (86)$$

$$\begin{aligned} \text{Diagram 2} &= -y_t^4 \left(\not{\int} \frac{1}{(K^2 + m_f^2)^2} + \dots \right) \int_x \Phi^\dagger \Phi \\ &= -y_t^4 \left\{ \frac{\mu^{-2\epsilon}}{(4\pi)^2} \left[\frac{1}{\epsilon} + \ln \frac{\bar{\mu}^2}{m_f^2} + \mathcal{O}(\epsilon) \right] + \frac{2}{(4\pi)^2} \ln \frac{m_f e^\gamma}{\pi T} - \frac{28\zeta(3)}{(4\pi)^4} \frac{m_f^2}{T^2} \dots \right\} \int_x \Phi^\dagger \Phi. \end{aligned} \quad (87)$$

The remaining diagrams are more involved but can be similarly computed by utilizing

$$\begin{aligned} \frac{x}{(x+a)^2(x+b)} &= \frac{a}{(a-b)(x+a)^2} + \frac{b}{(a-b)^2(x+a)} - \frac{b}{(a-b)^2(x+b)} \\ \frac{x^2}{(x+a)^2(x+b)^2} &= \frac{a^2}{(a-b)^2(x+a)^2} + \frac{b^2}{(a-b)^2(x+b)^2} + \frac{2ab}{(a-b)^3(x+a)} - \frac{2ab}{(a-b)^3(x+b)}. \end{aligned} \quad (88)$$

Considering only the non-derivative terms, they are, to the leading order in temperature,

given by

$$\begin{aligned}
\text{Diagram 1} &\simeq \frac{\lambda^2}{3} \int_x (\Phi^\dagger \Phi)^2 \not\int \frac{1}{(K^2 + m_h^2)^2} \\
&= -\frac{1}{2m_h} \left(-\frac{T}{4\pi} - \frac{4\mu^{-2\epsilon}}{(4\pi)^2} m_h \left[\ln \left(\frac{\bar{\mu} e^\gamma}{4\pi T} \right) + \frac{1}{2\epsilon} \right] + \frac{8\zeta(3)}{(4\pi)^4} \frac{m_h^3}{T^2} + \dots \right) \frac{\lambda^2}{3} \int_x (\Phi^\dagger \Phi)^2 \\
\text{Diagram 2} &\simeq -\frac{5}{8} g^4 \int_x (\Phi^\dagger \Phi)^2 \not\int \frac{K^2}{(K^2 + m_g^2)(K^2 + m_g^2)(K^2 + m_h^2)} \\
&\simeq -\frac{5}{8} g^4 \int_x (\Phi^\dagger \Phi)^2 \left\{ \left[\frac{T}{8\pi m_g} + \frac{2\mu^{-2\epsilon}}{(4\pi)^2} \left(\frac{1}{2\epsilon} + \ln \frac{\bar{\mu} e^{\gamma_E}}{4\pi T} \right) - \frac{4m_g^2 \zeta(3)}{(4\pi)^4 T^2} \right] \frac{-m_g^2}{m_h^2 - m_g^2} \right. \\
&\quad \left. + \left[-\frac{(m_g - m_h)T}{4\pi} - 2\frac{(m_g^2 - m_h^2)\mu^{-2\epsilon}}{(4\pi)^2} \left(\frac{1}{2\epsilon} + \ln \frac{\bar{\mu} e^{\gamma_E}}{4\pi T} \right) + 2\zeta(3) \frac{(m_g^4 - m_h^4)}{(4\pi)^4 T^2} \right] \frac{m_h^2}{(m_h^2 - m_g^2)^2} \right\} \\
\text{Diagram 3} &\simeq -\frac{3}{48} \lambda g^2 \int_x (\Phi^\dagger \Phi)^2 \not\int \frac{K^2}{(K^2 + m_g^2)(K^2 + m_h^2)(K^2 + m_h^2)} \\
&\simeq -\frac{3}{48} \lambda g^2 \int_x (\Phi^\dagger \Phi)^2 \left\{ \left[\frac{T}{8\pi m_h} + \frac{2\mu^{-2\epsilon}}{(4\pi)^2} \left(\frac{1}{2\epsilon} + \ln \frac{\bar{\mu} e^{\gamma_E}}{4\pi T} \right) - \frac{4m_h^2 \zeta(3)}{(4\pi)^4 T^2} \right] \frac{-m_h^2}{m_g^2 - m_h^2} \right. \\
&\quad \left. + \left[-\frac{(m_h - m_g)T}{4\pi} - 2\frac{(m_h^2 - m_g^2)\mu^{-2\epsilon}}{(4\pi)^2} \left(\frac{1}{2\epsilon} + \ln \frac{\bar{\mu} e^{\gamma_E}}{4\pi T} \right) + 2\zeta(3) \frac{(m_h^4 - m_g^4)}{(4\pi)^4 T^2} \right] \frac{m_g^2}{(m_g^2 - m_h^2)^2} \right\} \\
\text{Diagram 4} &\simeq \frac{g^4}{16} \int_x (\Phi^\dagger \Phi)^2 \not\int \frac{K^4}{(K^2 + m_h^2)(K^2 + m_h^2)(K^2 + m_g^2)(K^2 + m_g^2)} \\
&\simeq \frac{g^4}{16} \int_x (\Phi^\dagger \Phi)^2 \left\{ \frac{m_h^4}{(m_h^2 - m_g^2)^2} \left[\frac{T}{8\pi m_h} + \frac{2\mu^{-2\epsilon}}{(4\pi)^2} \left(\frac{1}{2\epsilon} + \ln \frac{\bar{\mu} e^{\gamma_E}}{4\pi T} \right) - \frac{4m_h^2 \zeta(3)}{(4\pi)^4 T^2} \right] \right. \\
&\quad + \frac{m_g^4}{(m_h^2 - m_g^2)^2} \left[\frac{T}{8\pi m_g} + \frac{2\mu^{-2\epsilon}}{(4\pi)^2} \left(\frac{1}{2\epsilon} + \ln \frac{\bar{\mu} e^{\gamma_E}}{4\pi T} \right) - \frac{4m_g^2 \zeta(3)}{(4\pi)^4 T^2} \right] \\
&\quad \left. + \frac{2m_h^2 m_g^2}{(m_h^2 - m_g^2)^3} \left[-\frac{(m_h - m_g)T}{4\pi} - \frac{2(m_h^2 - m_g^2)\mu^{-2\epsilon}}{(4\pi)^2} \left(\frac{1}{2\epsilon} + \ln \frac{\bar{\mu} e^{\gamma_E}}{4\pi T} \right) + \frac{2(m_h^4 - m_g^4) \zeta(3)}{(4\pi)^4 T^2} \right] \right\}. \tag{89}
\end{aligned}$$

3.2 Determination of m_g and m_f

It has been noted previously that certain 4-point amplitudes encounter infrared divergences when the gauge and fermion masses are taken to vanish. In the zero-T case, such a problem was not encountered when the gauge mass terms were not considered, as seen in the gauge-loop diagram in equation (50). It was unnecessary to explicitly separate out the vacuum expectation value ϕ_v from φ , and the renormalization factors Z for the coupling constants and fields of the unbroken action could be employed without any issue. However, for the Higgs sector, it was essential to focus on the proper Higgs mass term and consider the shift. This was because the goal was not the renormalization of the wrong-sign mass term, but rather that of the proper Higgs mass term of the broken-phase action. Consequently, the vacuum expectation value was separated out at the final stage, and the use of the massive Higgs propagator in the intermediate steps can be understood in this context. Similarly, in the finite-T case, a similar step is necessary for the Higgs sector. Additionally, it is

crucial to explicitly separate the vacuum expectation value of ϕ at the final stage even for the gauge and fermion sector analyses, but for a different reason: to remove the infrared divergences. Despite the apparent differences in approach between the zero-T and finite-T cases, the refined background field method (RBFM) in the spirit of Coleman-Weinberg provides a unified view, as stated in the introduction to the present section.

Now, let's examine how the mass terms m_g and m_f arise from thermal resummation. Specifically, we will consider the gauge and fermionic-loop diagrams in Fig. 5 (a) and (b), respectively. (The gauge case is slightly different in that the zero-T Higgs loop also gives rise to a mass term as we observed in section 2.1. However, this contribution is subleading and irrelevant.⁹) For the gauge loop diagram 5 (a), let's illustrate the idea with the $U(1)$ gauge field B_μ . The mass term arises from the coupling with the Higgs

$$-\frac{g'^2}{4}\Phi^\dagger\Phi B_\mu^2. \quad (90)$$

Note that the scalar field here is the background field Φ but not the quantum field ϕ . Once the field Φ develops a vev, that will lead to m_g . To obtain the precise expression of m_g , let us switch to the real basis and determine the vev of the scalar field. With thermal resummation in the scalar sector, the vacuum expectation value $\phi_v(T)$ is determined by

$$\frac{\partial}{\partial\phi}\left[-\frac{\lambda}{4!}\phi^4 + \frac{1}{2}m_\phi^2(T)\phi^2\right] = 0 \quad \Rightarrow \quad \phi_v(T) = \sqrt{\frac{6}{\lambda}} m_\phi(T) \quad (91)$$

where

$$m_\phi^2(T) \equiv \tilde{\mu}^2 - \frac{1}{12}\left[\lambda + \frac{3}{4}(3g^2 + g'^2) + 3y_t^2\right]T^2. \quad (92)$$

By substituting this into (90), one gets the expression for m_g . Considering the temperature that is substantially higher than the EW scale to which the renormalized mass parameter $\tilde{\mu}$ is set, $T \gg \tilde{\mu}$, the mass parameter $m_\phi(T)$ and $\phi_v(T)$ will be

$$m_\phi^2(T) \sim T^2 \quad , \quad \phi_v^2(T) \sim T^2. \quad (93)$$

Let us introduce a parameter c_g defined by

$$m_g(T) \equiv c_g T. \quad (94)$$

The parameter c_g is a function the coupling constants; in general it will also depend on one's renormalization scheme. For the fermionic diagram Fig. 5 (b) (we use the top quark sector to be specific), we view the Yukawa vertex

$$-y_t \bar{q} \tilde{\Phi} t_R + h.c. \quad (95)$$

⁹For the Linde problem, however, the analogous term from the fermionic loop should be relevant, as gluons do not couple to the Higgs. Therefore, the mass term from the fermion loop becomes the leading term. Additionally, if one neglects $\tilde{\mu}$, compared to the temperature-induced mass, then such terms become relevant.

as the mass term, treating $\tilde{\Phi}$ as a constant. Again, note that we use the background field $\tilde{\Phi}$ but not the quantum field $\tilde{\Phi}$. In terms of the complex scalar, the fermionic mass is given by $y_t \tilde{\Phi}$. At the final stage one will have to switch to the real basis. Then $\phi_v(T)$ emerges through $\tilde{\Phi}$; the fermionic mass term is $\frac{1}{\sqrt{2}} y_t \phi_v(T)$. We introduce a parameter c_f similarly to the gauge case:

$$m_f(T) \equiv c_f T. \quad (96)$$

By the same token one can introduce a parameter c_h :

$$m_h(T) \equiv c_h T. \quad (97)$$

With these definitions, the 4-pt functions previously calculated can be rewritten as

$$\begin{aligned}
\text{Sun} &= -\frac{3}{8} g^4 \left(-\frac{1}{4\pi c_g} - \frac{4\mu^{-2\epsilon}}{(4\pi)^2} \left[\ln \left(\frac{\bar{\mu} e^\gamma}{4\pi T} \right) + \frac{1}{2\epsilon} \right] + \frac{8\zeta(3)}{(4\pi)^4} c_g^2 + \dots \right) \int_x \Phi^\dagger \Phi \\
\text{Box} &= -y_t^4 \left\{ \frac{\mu^{-2\epsilon}}{(4\pi)^2} \left[\frac{1}{\epsilon} + \ln \frac{\bar{\mu}^2}{c_f^2 T^2} + \mathcal{O}(\epsilon) \right] + \frac{2}{(4\pi)^2} \ln \frac{c_f e^\gamma}{\pi} - \frac{28\zeta(3)}{(4\pi)^4} c_f^2 \dots \right\} \int_x \Phi^\dagger \Phi \\
\text{Bubble} &= -\frac{1}{2} \left(-\frac{1}{4\pi c_h} - \frac{4\mu^{-2\epsilon}}{(4\pi)^2} \left[\ln \left(\frac{\bar{\mu} e^\gamma}{4\pi T} \right) + \frac{1}{2\epsilon} \right] + \frac{8\zeta(3)}{(4\pi)^4} c_h^2 + \dots \right) \frac{\lambda^2}{3} \int_x (\Phi^\dagger \Phi)^2 \\
\text{Triangle} &\simeq -\frac{5}{8} g^4 \int_x (\Phi^\dagger \Phi)^2 \left\{ \left[\frac{1}{8\pi c_g} + \frac{2\mu^{-2\epsilon}}{(4\pi)^2} \left(\frac{1}{2\epsilon} + \ln \frac{\bar{\mu} e^{\gamma_E}}{4\pi T} \right) - \frac{4\zeta(3)}{(4\pi)^4} c_g^2 \right] \frac{-c_g^2}{c_h^2 - c_g^2} \right. \\
&\quad \left. + \left[-\frac{(c_g - c_h)}{4\pi} - 2 \frac{(c_g^2 - c_h^2) \mu^{-2\epsilon}}{(4\pi)^2} \left(\frac{1}{2\epsilon} + \ln \frac{\bar{\mu} e^{\gamma_E}}{4\pi T} \right) + 2\zeta(3) \frac{(c_g^4 - c_h^4)}{(4\pi)^4} \right] \frac{c_h^2}{(c_h^2 - c_g^2)^2} \right\} \\
\text{Triangle} &\simeq -\frac{3}{48} \lambda g^2 \int_x (\Phi^\dagger \Phi)^2 \left\{ \left[\frac{1}{8\pi c_h} + \frac{2\mu^{-2\epsilon}}{(4\pi)^2} \left(\frac{1}{2\epsilon} + \ln \frac{\bar{\mu} e^{\gamma_E}}{4\pi T} \right) - \frac{4\zeta(3)}{(4\pi)^4} c_h^2 \right] \frac{-c_h^2}{c_g^2 - c_h^2} \right. \\
&\quad \left. + \left[-\frac{(c_h - c_g)}{4\pi} - 2 \frac{(c_h^2 - c_g^2) \mu^{-2\epsilon}}{(4\pi)^2} \left(\frac{1}{2\epsilon} + \ln \frac{\bar{\mu} e^{\gamma_E}}{4\pi T} \right) + 2\zeta(3) \frac{(c_h^4 - c_g^4)}{(4\pi)^4} \right] \frac{c_g^2}{(c_g^2 - c_h^2)^2} \right\} \\
\text{Triangle} &\simeq \frac{g^4}{16} \int_x (\Phi^\dagger \Phi)^2 \left\{ \frac{c_h^4}{(c_h^2 - c_g^2)^2} \left[\frac{1}{8\pi c_h} + \frac{2\mu^{-2\epsilon}}{(4\pi)^2} \left(\frac{1}{2\epsilon} + \ln \frac{\bar{\mu} e^{\gamma_E}}{4\pi T} \right) - \frac{4\zeta(3)}{(4\pi)^4} c_h^2 \right] \right. \\
&\quad + \frac{c_g^4}{(c_h^2 - c_g^2)^2} \left[\frac{1}{8\pi c_g} + \frac{2\mu^{-2\epsilon}}{(4\pi)^2} \left(\frac{1}{2\epsilon} + \ln \frac{\bar{\mu} e^{\gamma_E}}{4\pi T} \right) - \frac{4\zeta(3)}{(4\pi)^4} c_g^2 \right] \\
&\quad \left. + \frac{2c_h^2 c_g^2}{(c_h^2 - c_g^2)^3} \left[-\frac{(c_h - c_g)}{4\pi} - \frac{2(c_h^2 - c_g^2) \mu^{-2\epsilon}}{(4\pi)^2} \left(\frac{1}{2\epsilon} + \ln \frac{\bar{\mu} e^{\gamma_E}}{4\pi T} \right) + \frac{2\zeta(3)}{(4\pi)^4} (c_h^4 - c_g^4) \right] \right\}. \quad (98)
\end{aligned}$$

In the fermion sectors, particularly for masses much smaller than the top quark mass, the values of c_f might be small. A small c_f results in a large logarithmic term in the fermion-loop diagram. It's anticipated that these large logarithmic terms can be managed through renormalization group techniques.

3.3 On the Linde problem

The thermal resummation approach outlined above offers insights into addressing the infrared problem known as the Linde problem. This issue arises from the absence of the magnetic thermal mass of the gauge fields in QCD. Consider eq. (30). Its finite-T counterpart is:

$$\begin{aligned}
\text{---}\bigcirc\text{---} &= -g^2\tilde{C}_2 \int\!\!\!\int \frac{\delta(P_1 + P_2)}{(K^2 + m_f^2) [(K - P_2)^2 + m_f^2]} \left[K \cdot A^a(P_1) (K - P_2) \cdot A^a(P_2) \right. \\
&\quad \left. + (K - P_2) \cdot A^a(P_1) K \cdot A^a(P_2) - K \cdot (K - P_2) A^a(P_1) \cdot A^a(P_2) \right] \\
&= -g^2\tilde{C}_2 \int\!\!\!\int \frac{K^\mu(K - P_2)^\nu + (K - P_2)^\mu K^\nu - K^\rho(K - P_2)_\rho \delta_{\mu\nu}}{(K^2 + m_f^2) [(K - P_2)^2 + m_f^2]} A_\mu^a A_\nu^a \delta(\Sigma P).
\end{aligned} \tag{99}$$

By focusing on the P -independent terms, one gets

$$\begin{aligned}
&\Rightarrow -g^2\tilde{C}_2 \int\!\!\!\int \frac{2K^\mu K^\nu - K^2\delta_{\mu\nu}}{(K^2 + m_f^2)^2} \\
&= g^2\tilde{C}_2 \left\{ \left[\delta_{\mu 0}\delta_{\nu 0} + \left(1 - \frac{2}{d}\right)\delta_{\mu i}\delta_{\nu i} \right] \int\!\!\!\int \frac{K^2}{(K^2 + m_f^2)^2} + \left[-2\delta_{\mu 0}\delta_{\nu 0} + \frac{2}{d}\delta_{\mu i}\delta_{\nu i} \right] \int\!\!\!\int \frac{k_n^2}{(K^2 + m_f^2)^2} \right\}.
\end{aligned} \tag{100}$$

One can show

$$\int\!\!\!\int \frac{K^2}{(K^2 + m_f^2)^2} = \tilde{I}(m_f, T) + \frac{m_f}{2} \frac{\partial}{\partial m_f} \tilde{I}(m_f, T). \tag{101}$$

Since the mass depends on the temperature, $m_f = m_f(T)$, care is required when taking $\frac{\partial}{\partial T}$ on $\tilde{I}(m, T)$. One can also show

$$\int\!\!\!\int \frac{k_n^2}{(K^2 + m_f^2)^2} = \frac{1}{2}\tilde{I}(m_f, T) - \frac{T}{2} \frac{\partial}{\partial T} \tilde{I}(m_f, T) + \frac{T}{4m_f} \left(\frac{\partial m_f^2}{\partial T} \right) \frac{\partial}{\partial m_f} \tilde{I}(m_f, T). \tag{102}$$

Substituting these into (100) one gets

$$\begin{aligned}
&-g^2\tilde{C}_2 \int\!\!\!\int \frac{2K^\mu K^\nu - K^2\delta_{\mu\nu}}{(K^2 + m_f^2)^2} \\
&= g^2\tilde{C}_2 \left\{ \delta_{\mu 0}\delta_{\nu 0} \left[T \frac{\partial}{\partial T} \tilde{I} + \frac{m_f}{2} \frac{\partial}{\partial m_f} \tilde{I} - T \left(\frac{\partial m_f}{\partial T} \right) \frac{\partial}{\partial m_f} \tilde{I} \right] \right. \\
&\quad \left. + \frac{1}{3}\delta_{\mu i}\delta_{\nu i} \left(2\tilde{I} - T \frac{\partial}{\partial T} \tilde{I} + \frac{m_f}{2} \frac{\partial}{\partial m_f} \tilde{I} + T \left(\frac{\partial m_f}{\partial T} \right) \frac{\partial}{\partial m_f} \tilde{I} \right) \right\}.
\end{aligned} \tag{103}$$

The explicit expression can be straightforwardly found by substituting $\tilde{C}_2 = 2$, \tilde{I} , $\frac{\partial}{\partial T} \tilde{I}$, and $\frac{\partial}{\partial m_f} \tilde{I}$. The coefficient of $\delta_{\mu i}\delta_{\nu i}$ no longer vanishes, which implies the presence of magnetic thermal mass.

3.4 time-dependent temperature and a curved background

In order to achieve a more comprehensive understanding of early Universe physics, particularly in relation to the cosmological constant problem and the Hubble tension, it is imperative to develop a formalism for quantum gravitational thermodynamics. Such a formalism should account for both quantum effects and finite-temperature effects. In this section, we contemplate the methodology for conducting time-dependent finite-temperature analysis within a FLRW background.

While there are circumstances where higher-derivative quantum-correction terms cannot be disregarded [30, 31], the present case is likely one where the leading-order action suffices for cosmological purposes. Contributions of gravitons are expected to be small and unlikely to alter the qualitative features observed so far. Nonetheless, it's beneficial to consider how to undertake time-dependent finite-temperature quantum-gravitational perturbation theory to ensure the validity of subsequent discussions.

The FLRW spacetime background introduces nontrivial technical challenges: it is both curved and has a time-dependent temperature. As for the complications of a curved background at zero-T, an effective method for calculating curved-spacetime Feynman diagrams has been devised [16]. Another major obstacle is how to perform quantum gravitational thermodynamics. While a full solution to these problems won't be pursued here, we propose a prescription that seems natural and readily applicable - which also seems promising for the perspective of a full solution - to relatively simple spacetimes like the FLRW universe. The primary tool is again the general form of the propagator obtained in previous work [16]. By employing this tool, the analysis is simplified to calculating diagrams in a constant-temperature flat-spacetime background.

Our thermodynamics prescription is based on the well-known equilibrium form of the density operator. Several justifications support using this form here. Firstly, although the Universe was not always in equilibrium, it was so for most of its history. Even when it was not in equilibrium, equilibrium thermodynamics often provides a good approximation. Secondly, it's plausible to extend the definition of temperature (and equilibrium) to a more general notion, such as time- and/or space-dependent temperature. Evidently, the temperature of the FLRW background varies with time. (Position-dependent temperature was also introduced in the literature.) Furthermore, it's possible to have a nontrivial temperature for a wide range of spacetimes, as temperature can be introduced as a Lagrange multiplier in entropy maximization procedures [32].

With these considerations, we extend the constant finite-temperature formalism to the time-dependent case by replacing the constant temperature in the Euclidean-time integral with a time-dependent one, scaling as $T(t) \sim \frac{1}{a(t)}$, where a denotes the scale parameter. To illustrate this, let us review the zero-temperature curved-spacetime Feynman diagram analysis by focusing on the metric. We split the metric into solution background and quantum fluctuation components:

$$g_{\mu\nu} \rightarrow h_{\mu\nu} + g_{s\mu\nu} \tag{104}$$

where $g_{s\mu\nu}$ denote the classical solutions and $h_{\mu\nu}$ the fluctuation fields.¹⁰ The zero-temperature

¹⁰For the sake of simplicity in our discussion, we will omit the consideration of the background field, which

loop analysis is based on the following two-point function (see [14] for the conventions):

$$\langle h_{\mu\nu}(x)h_{\rho\sigma}(y) \rangle = P_{\mu\nu\rho\sigma} \Delta(x-y) \quad (105)$$

where the tensor $P_{\mu\nu\rho\sigma}$ is given, in de Donder gauge, by [10]

$$P_{\mu\nu\rho\sigma} \equiv \frac{\bar{\kappa}^2}{2} \left(g_{s\mu\rho}g_{s\nu\sigma} + g_{s\mu\sigma}g_{s\nu\rho} - \frac{1}{2}g_{s\mu\nu}g_{s\rho\sigma} \right); \quad (106)$$

where $\bar{\kappa}^2 \equiv 2\kappa^2$; $\Delta(x-y)$ is Green's function for a massless scalar theory¹¹:

$$\Delta(x-y) = \int \frac{d^4k}{(2\pi)^4} \frac{1}{\sqrt{-g_s(x)}} \frac{e^{ik \cdot (x-y)}}{ik_\mu k_\nu g_s^{\mu\nu}(x)}. \quad (107)$$

The propagator can then be transformed as follows: defining the “flattened” momentum and coordinates, (\tilde{k}, \tilde{x}) , as

$$\tilde{k}_{\underline{\alpha}} \equiv e_{s\underline{\alpha}}^\mu k_\mu \quad , \quad \tilde{x}^{\underline{\beta}} \equiv e_{s\underline{\nu}}^\beta x^\nu \quad , \quad e_{s\underline{\alpha}}^\mu e_{s\underline{\beta}}^\nu g_{s\mu\nu} = \eta_{\underline{\alpha}\underline{\beta}} \quad (108)$$

where the underlined indices denote the flattened ones, one gets the flattened propagator:

$$\Delta(\tilde{x} - \tilde{y}) = \int \frac{d^4\tilde{k}}{(2\pi)^4} \frac{e^{i\tilde{k} \cdot (\tilde{x} - \tilde{y})}}{i\tilde{k}_{\underline{\alpha}} \tilde{k}_{\underline{\beta}} \eta^{\underline{\alpha}\underline{\beta}}}. \quad (109)$$

With this, the steps for evaluating Feynman diagrams in a curved spacetime become parallel to those for the flat case.

Considering the time-dependent temperature in a FLRW background, although $T(t)$ is not constant, it is covariantly constant. This is because the time-dependence of $T(t)$ comes from $a(t)$, which is a metric component and is thus annihilated by a covariant derivative. In the usual comoving coordinates, the mode associated with the time-direction takes $\omega_n = 2\pi T(t)n$. By introducing “flattened” coordinates of the comoving coordinates, the time-dependent-T curved-spacetime analysis parallels that of the constant-T flat-spacetime, with all curvature effects included in the formalism. However, there remains some arbitrariness associated with choosing the finite parts, akin to the usual infinities in quantum field theory. Detailed analysis of loops involving the SM fields and gravitons will demand extensive and intensive efforts and warrants dedicated research.

4 Implications for cosmology

With the UV and IR divergences at finite temperature duly addressed, let us look into the cosmological implications of our findings, focusing on the cosmological constant (CC) problem and the Hubble tension. We consider the leading part of the 1PI effective action in the

would be the metric analog of ϕ_B ; the discussion can be extended to include it.

¹¹If one views the CC term as contributing to the graviton mass, $\Delta(x-y)$ should be taken as the propagator of a massive scalar theory.

derivative expansion coupled with conventional hydrodynamic or kinetic-theory matter. The hydrodynamic matter field equations, i.e., the conservation equations, remain unchanged. As for the field equations of Standard Model matter, we set all, except the Higgs, of the fields to zero. In both the metric field equation and the SM matter field equations, various coupling constants are replaced by their T -dependent effective counterparts.

The essence of our analysis regarding the finite-temperature effects on the CC problem was previously presented in our works [16, 17]. In those studies, employing an Einstein-scalar system, we demonstrated that the CC problem transitions from an order-60 problem to an order-4 problem. It was anticipated that the inclusion of SM matter fields would further narrow this order gap. We provide a detailed explanation here. Regarding the Hubble tension, there are several factors that deviate the system from conventional treatments. Most notably, the effective coupling constants appearing in the field equations are all temperature-dependent, hence time-dependent.

4.1 Cosmological constant problem

In [16, 17], a potential solution to the CC problem was explored by introducing a novel renormalization scheme. One crucial aspect was setting the renormalized mass of the scalar field to the order of the Cosmic Microwave Background temperature. However, there were some loose ends in the analysis. Firstly, the extension of the results from constant temperature QFT analysis to a time-dependent temperature scenario lacked rigorous treatment of the time-dependent finite- T QFT procedure. This gap has been addressed in the previous section. Secondly, there remained a significant factor of $\sim 10^4$ or 10^5 difference between the observed and theoretical values. As anticipated, this discrepancy should be partly attributed to the fact that the system considered there was an Einstein-scalar system. Here, we confirm that the inclusion of SM particle content further narrows this gap. As mentioned in section 3.4, one can consider a flat background and constant temperature. (The result for the FLRW spacetime is obtained simply by replacing $T \rightarrow \frac{T}{a^4}$ at the end.)

In the previous work, the comparison between the observed value and theoretical one was made in the energy (GeV) unit. Here, we repeat the comparison, but the comparison will be made in the $[L]^{-4}$ unit for a cross-check. The observed value of the vacuum energy density is

$$\rho_\Lambda \approx 3.7 \times 10^9 \text{ eV} m^{-3}. \quad (110)$$

One can go from GeV to m by the relation (see, e.g., [33])

$$GeV = 0.5 \times 10^{14} \text{ cm}^{-1} = 0.5 \times 10^{16} \text{ m}^{-1} \quad (111)$$

from which one gets

$$\rho_\Lambda \approx 3.7 \times 10^9 \times 0.5 \times 10^7 m^{-4} \approx 10^{16} m^{-4}. \quad (112)$$

Let us compare this with the theoretical value based on our proposal. The temperature is 2.7 K and

$$1 \text{ K} = 8.6 \times 10^{-14} \text{ GeV} = 8.6 \times 10^{-14} \times 0.5 \times 10^{16} \text{ m}^{-1} = 4 \times 10^2 \text{ m}^{-1}. \quad (113)$$

Since the temperature-dependent CC term scales as $\sim T^4$,¹² one gets, for the present CC,

$$\sim (2.75K)^4 \approx 10^{12} m^{-4}, \quad (114)$$

thus the gap between the experimental and theoretical values is on the order 10^4 or so.

As anticipated in [16], the SM particle content should further reduce the gap. When counting the number of fermionic degrees of freedom, there is a delicate point to consider. The total number of fermionic degrees of freedom depends on whether neutrinos are treated as Dirac spinors or Majorana spinors. In this work, we treat them as Dirac spinors. Since our interest lies in the order of magnitude of the CC, our qualitative conclusion remains unchanged even if neutrinos are treated as Majorana spinors.¹³ Here's how the counting goes: for a Dirac spinor, which has 4 components, the result of its one-loop contribution to the free energy density is given by

$$-4 \int \frac{1}{2} \ln(K^2 + m_f^2) + (\text{irrelevant constant}). \quad (115)$$

As we have reviewed in the previous section,

$$\int \frac{1}{2} \ln(K^2 + m_f^2) = \frac{7}{8} \frac{\pi^2}{90} T^4 + \dots . \quad (116)$$

For the quarks, the counting is $3 \times 3 \times 4 \times 2 = 72$, where the 3's come from the colors and flavors. The factor 4 arises from Eq. (115), and the last factor 2 stems from considering both the left-handed and right-handed quarks as "doubles" in the counting. Similarly, when counting the contributions from charged leptons, the total count is $72 + 12 = 84$.

Suppose we treat the neutrinos as Dirac spinors. Since there are six of them, the count adds up to 6, resulting in a grand total of $84 + 12 = 96$. However, if we treat them as Majorana spinors, the count becomes $84 + 6 = 90$.¹⁴ These contributions, with a weight of $\frac{7}{8}$, should be added to the contribution from the 28 bosonic degrees of freedom, each with a weight of 1. With this total, the CC problem is reduced from a 10^{60} -order problem to a $10^2 - 10^3$ -order problem.

Now, let's pause and reassess the renormalization of the cosmological constant. The component we've been considering is the one-loop correction, and we've demonstrated that it is two or three orders of magnitude smaller than the observed value. However, it's important to remember that we can introduce a classical piece to the CC. It's not out of the norm but well within the standard practice of renormalization procedure to introduce a classical term, i.e., the renormalized CC, that is two or three orders of magnitude larger than the one-loop quantum corrections. In other words, we no longer face the unnaturalness, the CC problem, of dealing with adding and/or subtracting extremely large and small numbers.

¹²The reason for employing a high-T expansion despite the fact that the CMB temperature is considered was explained in [16].

¹³For a Majorana spinor, going from Minkowski spacetime to Euclidean spacetime involves doubling of degrees of freedom. An Euclideanization method that avoids this doubling was proposed in the past; for instance, see [34].

¹⁴Strictly speaking, one would also have to consider the graviton contributions of two physical states, to be precise.

4.2 Effective constants, Hubble tension, and CC non-conservation

Another potentially significant cosmological implication of our present results concerns the Hubble tension. The conventional Standard Model of cosmology utilizes a classical Einstein system coupled with kinetic-theory matter. However, we propose a more general approach where we consider a finite-temperature system comprising two components: the first component is the leading-order effective action of the Standard Model coupled with gravity, and the second component is the hydrodynamic or kinetic matter system coupled to the first. In finding solutions to the field equations, all of the Standard Model field vacuum expectation values except that of the Higgs field can be set to zero.

Compared with the conventional Standard Model of cosmology, our approach incorporates several additional effects. Most notably, our system includes finite-temperature quantum-field-theoretic effects, whereas in the conventional analysis, only the thermodynamics of the kinetic matter is considered. The consequential main difference in our approach is that all coupling constants, including the cosmological constant (CC) and Newton's constant, are replaced by temperature-dependent effective ones. Recall the renormalization method employed in our work, which is essentially the \overline{MS} scheme. Thus, the renormalization group running of the fundamental coupling constants remains the same as that of the zero-temperature theory. However, the coupling constants appearing in the action or field equations used in cosmology are the effective ones.

Let's examine the CC and Einstein-Hilbert sector to scrutinize the potential implications of the effective coupling constants for Hubble tension. Consider the metric field equation:

$$R_{\mu\nu} - \frac{1}{2}g_{\mu\nu}R + \Lambda_{eff}(t) g_{\mu\nu} = 8\pi G_{eff}(t) T_{\mu\nu} \quad (117)$$

where $T_{\mu\nu}$ contains all of the matter sectors. In the conventional analysis, both effective couplings Λ_{eff} and G_{eff} are treated as constants. Since they are now time-dependent, it is natural to expect that their presence will modify the best fit cosmological parameters of the CMB power spectrum.

A perhaps more profound potential implication of the time-dependent effective coupling constants is for non-conservation of the vacuum energy. Taking a divergence on both sides and substituting

$$\nabla^\mu (R_{\mu\nu} - \frac{1}{2}g_{\mu\nu}R) = 0 \quad (118)$$

where the covariant derivative is one associated with quantum-corrected metric, and¹⁵

$$\nabla^\mu T_{\mu\nu} = 0 \quad (119)$$

one gets

$$\nabla_\nu \Lambda_{eff}(t) = 8\pi T_{\mu\nu} \nabla^\mu G_{eff}(t). \quad (120)$$

Note that the (non)constancy of Λ_{eff} and G_{eff} is interconnected: if Λ_{eff} were a constant, it implies that the right-hand side vanishes (hence the constancy of G_{eff}), and this equation

¹⁵For a more general case, see the conclusion.

can be interpreted as conservation of vacuum energy. However, the non-constancy of Λ_{eff} , implies that the vacuum energy, unlike the matter or radiation sector, is not conserved. In particular, the effect feeds back to the Newton's constant. We will discuss this further in the conclusion.

5 Conclusion

In this work, we have brought forth a unified technical framework provided by RBFM and analyzed the Standard Model coupled to dynamic gravity in a FLRW background. Several technical hurdles have been overcome. Firstly, we addressed the IR divergences by employing thermal resummation not only in the scalar sector but also in the gauge and fermionic sectors. We have highlighted that this procedure allows one to avoid the Linde problem. Secondly, progress has been made on how to perform finite-T QFT with time-dependent temperature. This problem may be considered in the context of more general spacetimes: by employing "flat" coordinates, the analysis becomes analogous to that of a flat spacetime.¹⁶

Our method is optimized for computing the 1PI effective action. For illustrations, we computed several sectors of the effective action, including the Higgs sector. The temperature-dependent terms are ubiquitous and call for consideration in cosmology. For cosmological applications, the leading order of the effective action should be sufficient. It should then be coupled to the hydrodynamic or kinetic matter system. It was noted in an \overline{MS} renormalization scheme that the effective coupling constants appearing in the cosmological Lagrangian are all temperature-, thus time-, dependent, although the fundamental coupling constants still have the same renormalization group flow as in the zero-T case.

Two cosmological applications were considered: the CC problem and Hubble tension. By tightening a couple of loose ends in the earlier analysis in [16] [17], we have observed that one no longer encounters the need for fine-tuning: the one-loop correction is smaller than the observed value of the CC by a few orders. It is not unnatural to introduce a classical piece of the CC that is a few orders larger than the one-loop result. The appearance of the effective coupling constants should definitely have some impact on analyses, such as the CMB power spectrum. As a preliminary discussion, we have pointed out that the temperature effects have the potential to ameliorate Hubble tension. More profoundly, the "conservation law" given in (120) may well signify certain mysterious aspects of our Universe.

There are several future directions worth pursuing.

Perhaps the most urgent direction is to analyze the finite-T effects on cosmological parameters, particularly the Hubble parameter. Currently, work is underway to numerically study these effects. Preliminary results indicate that the present-time Hubble constant is significantly influenced by the temperature-dependent part of the CC. Additionally, it will be fascinating to explore the intriguing aspect of the temperature effect observed at the end

¹⁶Relatedly, more work is needed to generalize the concept of equilibrium: temperature can be introduced as a Lagrange multiplier, which need not necessarily be a constant in general. One could argue that the Lagrange multiplier assumes the role of temperature at equilibrium. It appears that temperature can be defined more broadly beyond the standard notion of equilibrium.

of section 4.2: the constraint between the renormalization of the CC and Newton's constant. In standard cosmology, separate conservation of each matter sector is enforced. Genuine constancy of the CC trivially satisfies this requirement. However, as observed at the end of section 4.2, the time dependence of the CC deviates from this, which, in turn, should have cosmological implications on other matter sectors through gravitational interactions. One can extend the non-conservation of the CC further in a more general context. In [35], it was noted that a Noether current fails to be conserved, meaning it takes on a different form, when a Neumann boundary condition is applied. Similarly, one could extend this observation to the level of equations of motion: relaxing the requirement for separate conservation allows for the consideration of non-conservation in at least some of the matter components.

Another direction, although less urgent, is to gather more examples demonstrating the compatibility of different renormalization schemes. While the finite renormalization-group invariance of physical quantities ensures this compatibility, explicitly demonstrating it would be worthwhile.

References

- [1] J. I. Kapusta and C. Gale, “Finite-Temperature Field Theory: Principles and Applications,” Cambridge university press (2006)
- [2] M. Le Bellac, “Thermal Field Theory,” Cambridge university press (2000)
- [3] M. Laine and A. Vuorinen, “Basics of Thermal Field Theory,” Lect. Notes Phys. **925**, pp.1-281 (2016) doi:10.1007/978-3-319-31933-9 [arXiv:1701.01554 [hep-ph]].
- [4] P. Langacker, ”The Standard Model and beyond,” 2nd ed., CRC press (2017)
- [5] M. D. Schwartz, ”Quantum field theory and the Standard Model,” Cambridge university press (2014)
- [6] S. Weinberg, “Cosmology,” Oxford university press (2008).
- [7] S. Dodelson and F. Schmidt, “Modern Cosmology,” Academic press (2021).
- [8] D. Baumann, “Cosmology,” Cambridge university press (2022).
- [9] I. Y. Park, “Hypersurface foliation approach to renormalization of ADM formulation of gravity,” Eur. Phys. J. C **75**, no.9, 459 (2015) doi:10.1140/epjc/s10052-015-3660-x [arXiv:1404.5066 [hep-th]].
- [10] I. Y. Park, “Lagrangian constraints and renormalization of 4D gravity,” JHEP **04**, 053 (2015) doi:10.1007/JHEP04(2015)053 [arXiv:1412.1528 [hep-th]].
- [11] I. Y. Park, “Four-Dimensional Covariance of Feynman Diagrams in Einstein Gravity,” Theor. Math. Phys. **195**, no.2, 745-763 (2018) doi:10.1134/S0040577918050094 [arXiv:1506.08383 [hep-th]].
- [12] I. Y. Park, “One-loop renormalization of a gravity-scalar system,” Eur. Phys. J. C **77**, no.5, 337 (2017) doi:10.1140/epjc/s10052-017-4896-4 [arXiv:1606.08384 [hep-th]].
- [13] I. Y. Park, “Revisit of renormalization of Einstein-Maxwell theory at one-loop,” PTEP **2021**, no.1, 013B03 (2021) doi:10.1093/ptep/ptaa167 [arXiv:1807.11595 [hep-th]].
- [14] I. Park, “Foliation-Based Approach to Quantum Gravity and Applications to Astrophysics,” Universe **5**, no.3, 71 (2019) doi:10.3390/universe5030071 [arXiv:1902.03332 [hep-th]].
- [15] C. Ford, I. Jack and D. R. T. Jones, “The Standard model effective potential at two loops,” Nucl. Phys. B **387**, 373-390 (1992) [erratum: Nucl. Phys. B **504**, 551-552 (1997)] doi:10.1016/0550-3213(92)90165-8 [arXiv:hep-ph/0111190 [hep-ph]].
- [16] I. Y. Park, “Cosmological constant as a finite temperature effect,” Int. J. Mod. Phys. A **37**, no.27, 2250173 (2022) doi:10.1142/S0217751X22501731 [arXiv:2101.02297 [hep-ph]].

- [17] I. Y. Park, “Quantization of Gravity and Finite Temperature Effects,” *Particles* **4**, no.4, 468-488 (2021) doi:10.3390/particles4040035 [arXiv:2109.01647 [hep-th]].
- [18] J. Solà Peracaula, “Cosmological constant and vacuum energy: old and new ideas,” *J. Phys. Conf. Ser.* **453**, 012015 (2013) doi:10.1088/1742-6596/453/1/012015 [arXiv:1306.1527 [gr-qc]].
- [19] C. Balazs, “Observable vacuum energy is finite in expanding space,” [arXiv:2203.16753 [gr-qc]].
- [20] P. M. Stevenson, “Optimized Perturbation Theory,” *Phys. Rev. D* **23**, 2916 (1981) doi:10.1103/PhysRevD.23.2916
- [21] M. Sher, “Electroweak Higgs Potentials and Vacuum Stability,” *Phys. Rept.* **179**, 273-418 (1989) doi:10.1016/0370-1573(89)90061-6
- [22] A. G. Riess, L. M. Macri, S. L. Hoffmann, D. Scolnic, S. Casertano, A. V. Filippenko, B. E. Tucker, M. J. Reid, D. O. Jones and J. M. Silverman, *et al.* “A 2.4% Determination of the Local Value of the Hubble Constant,” *Astrophys. J.* **826**, no.1, 56 (2016) doi:10.3847/0004-637X/826/1/56 [arXiv:1604.01424 [astro-ph.CO]].
- [23] V. Poulin, T. L. Smith, T. Karwal and M. Kamionkowski, “Early Dark Energy Can Resolve The Hubble Tension,” *Phys. Rev. Lett.* **122**, no.22, 221301 (2019) doi:10.1103/PhysRevLett.122.221301 [arXiv:1811.04083 [astro-ph.CO]].
- [24] H. Moshafi, H. Firouzjahi and A. Talebian, “Multiple Transitions in Vacuum Dark Energy and H_0 Tension,” *Astrophys. J.* **940**, no.2, 121 (2022) doi:10.3847/1538-4357/ac9c58 [arXiv:2208.05583 [astro-ph.CO]].
- [25] A. D. Linde, “Infrared Problem in Thermodynamics of the Yang-Mills Gas,” *Phys. Lett. B* **96**, 289-292 (1980) doi:10.1016/0370-2693(80)90769-8
- [26] J. Ghiglieri, A. Kurkela, M. Strickland and A. Vuorinen, “Perturbative Thermal QCD: Formalism and Applications,” *Phys. Rept.* **880**, 1-73 (2020) doi:10.1016/j.physrep.2020.07.004 [arXiv:2002.10188 [hep-ph]].
- [27] M. E. Machacek and M. T. Vaughn, “Two Loop Renormalization Group Equations in a General Quantum Field Theory. 3. Scalar Quartic Couplings,” *Nucl. Phys. B* **249**, 70-92 (1985) doi:10.1016/0550-3213(85)90040-9
- [28] Y. F. Pirogov and O. V. Zenin, “Two loop renormalization group restrictions on the standard model and the fourth chiral family,” *Eur. Phys. J. C* **10**, 629-638 (1999) doi:10.1007/s100520050602 [arXiv:hep-ph/9808396 [hep-ph]].
- [29] P. B. Arnold and O. Espinosa, “The Effective potential and first order phase transitions: Beyond leading-order,” *Phys. Rev. D* **47**, 3546 (1993) [erratum: *Phys. Rev. D* **50**, 6662 (1994)] doi:10.1103/PhysRevD.47.3546 [arXiv:hep-ph/9212235 [hep-ph]].

- [30] A. J. Nurbagambetov and I. Y. Park, “Quantum-induced trans-Planckian energy near horizon,” *JHEP* **05**, 167 (2018) doi:10.1007/JHEP05(2018)167 [arXiv:1804.02314 [hep-th]].
- [31] A. J. Nurbagambetov and I. Y. Park, “Quantum-Gravitational Trans-Planckian Radiation by a Rotating Black Hole,” *Fortsch. Phys.* **69**, no.10, 2100064 (2021) doi:10.1002/prop.202100064 [arXiv:2007.06070 [hep-th]].
- [32] J. J. Sakurai, “Modern Quantum Mechanics,” The Benjamin/Cummings Publishing Company (1985)
- [33] Dmitry S Gorbunov and Valery A Rubakov, ”Introduction to the theory of the early universe: Hot Big Bang theory,” World Scientific (2011)
- [34] P. van Nieuwenhuizen and A. Waldron, *Phys. Lett. B* **389**, 29-36 (1996) doi:10.1016/S0370-2693(96)01251-8 [arXiv:hep-th/9608174 [hep-th]].
- [35] I. Y. Park, “Boundary dynamics in gravitational theories,” *JHEP* **07**, 128 (2019) doi:10.1007/JHEP07(2019)128 [arXiv:1811.03688 [hep-th]].